Master's Thesis

Molecular Dynamics Simulations of Silver-induced Crystallization in Silicon Nanocluster

Junlei Zhao
2013

Supervisor: Doctor Flyura Djurabekova
Examiners: Professor Kai Nordlund
Doctor Flyura Djurabekova

UNIVERSITY OF HELSINKI
DEPARTMENT OF PHYSICS

P.O. Box 64 (Gustaf Hällströmin katu 2a)
00014 University of Helsinki

HELSINGIN YLIOPISTO
HELSINGFORS UNIVERSITET
UNIVERSITY OF HELSINKI

Tiedekunta – Fakultet – Faculty	Laitos – Institution– Department	
Faculty of Science	Department of Physics	
Tekijä – Författare – Author		
Junlei Zhao		
Työn nimi – Arbetets titel – Title		
Molecular Dynamics Simulations of Silver-induced Crystallization in Silicon Nanocluster		
Oppiaine – Läroämne – Subject		
Computational Nanoscience and Matrials Physics		
Työn laji – Arbetets art – Level	Aika – Datum – Month and year	Sivumäärä – Sidoantal – Number of pages
Master's Thesis	Dec 2012	42

Tiivistelmä – Referat – Abstract

Metal-induced crystallization (MIC) has been investigated extensively as an alternative crystallization process in the silicon based photovoltaic industry. In this work, we simulate a nanoscale version of this process by using molecular dynamics simulation involving liquid Si nanoclusters inoculated with Ag atoms in Ar thermal bath. The simulations reveal that the energy released during coalescence of the silver silicide region is the main factor to remelt the surface of the Si nanocluster.

In an earlier report, Ag nanoparticles is observed to induced crystallization in 12-15 nm-diameter silicon cluster, which upon further cooling results in nano-polycrystalline silicon core and segregated Ag sub-shells. The work focuses on the crucial conditions that influence the MIC process, such as (i) number of Ag atoms per unit volume, (ii) initial temperature of Si cluster, (iii) crystallization temperature and (iv) cooling rate of the Si cluster. The results presented in this study provide insight into the effect of the first three parameters. Also, the results suggest that the coalescence of eutectic phase is the essential step which induces the crystallization.

Avainsanat – Nyckelord – Keywords

MD simulations, metal-induced crystallization, Ag, Si, nanocluster

Ohjaaja tai ohjaajat – Handledare – Supervisor or supervisors

Doctor Flyura Djurabekova and Professor Kai Nordlund

Säilytyspaikka – Förvaringställe – Where deposited

Muita tietoja – Övriga uppgifter – Additional information

Contents

1 Introduction

The conceptual origins of nanoscience and nanotechnology can be traced back to December 29, 1959, when Richard Feynman gave the lecture "There's Plenty of Room at the Bottom" at Caltech, USA. He described a field which is "not quite the same as the others in that it will not tell us much of fundamental physics but it is more like solid-state physics in the sense that it might tell us much of great interest about the strange phenomena that occur in complex situations." This simple inspiring idea has often been referred to as the first "seed" of one of the most promising interdisciplinary branches of science.

In 1974, the Japanese scientist Norio Taniguchi used the term "nano-technology" at a conference [1]. Research in nanoscience rapidly developed in the 1980s with the invention of the scanning tunnelling microscope (STM)[2] in 1981 and the discovery of fullerenes in 1985[3]. Soon after, K. Eric Drexler published his book *Engines of Creation: The Coming Era of Nanotechnology* in 1986, in which he proposed the idea of a nanoscale assembler which would be able to build a copy of itself and other items of arbitrary complexity. Although Drexler's vision is still far from realization with today's technology, this idea is regarded as the foundation of "molecular nanotechnology" or "molecular manufacturing".

The definition of nanoscience has several conventions, but each description has certain criteria in common: (1) the system studied has at least one dimension within 1 100 nm; (2) some properties of the system are different from the corresponding macroscopic system. For instance, the melting temperature of silicon nanoclusters is a linear function of $N^{-1/3}$ (where N is the number of atoms), as shown in Figure 1. Additionally, the melting temperature relies on the heating rate, which is not the case for bulk silicon.

Research in nanoscience is mostly done both experimentally and by meanS of computer simulations. Experimental methods include the fabrication of nanostructures and examination of their properties, which would be very difficult and expensive to realize. Moreover, the accuracy of the results is limited by sample imperfections and the feasibility of the experimental instruments. For these reasons, computer simulations are used to study the properties of nanosystems. Computer simulations have several highly desirable features: (1) they are able to study the transformation process from an extremely short period (nanoseconds) to very long time scales (even years) and (2) to reproduce conditions and interactions within a certain level of precision (usually large systems and long time scales use crude approximations); (3) they are also relatively cheap compared to experimental methods. The limitations of computer simulations are that the real conditions and interactions can be very expensive to be replicated perfectly. Therefore, the simulations will not be ex-

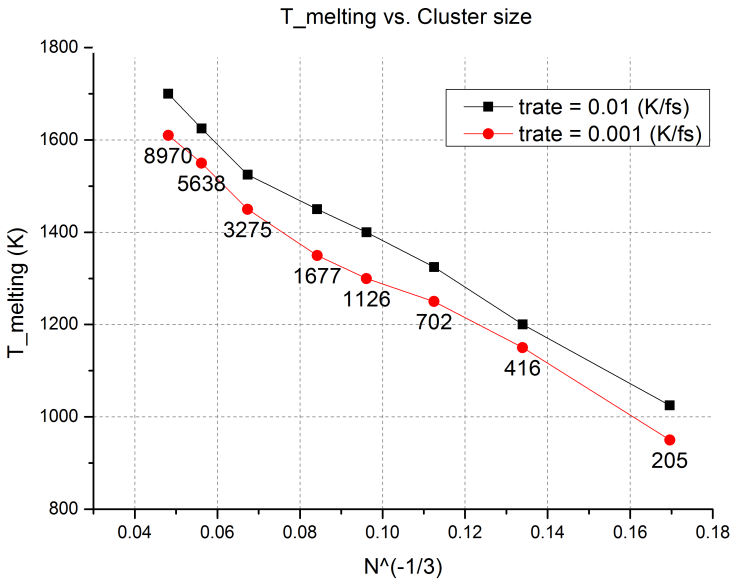

Figure 1: Dependence of melting temperature on cluster size and heating rate. Results from simulations done in the current work.

actly identical to the experimental process. If the process is simulated as exactly as possible, the computational cost increases dramatically with the precision. Many models have been developed over the past thirty years, from finding exact solutions to SchrÃ¶dinger equation (which is impossible analytically in many-body systems) to Monte Carlo simulations. As shown in Figure 2, molecular dynamics is suitable for simulating systems which contain more than 10^3 atoms. Density functional theory and other quantum mechanical methods are usually applied for systems with less than 100 atoms.

In this work, the silver-induced crystallization of silicon nanoclusters is investigated by means of molecular dynamics simulations. An overview of basic information about nanoclusters is given in Section 2. Previous studies on metal-induced crystallization are reviewed in Section 3. The simulation method is described in Section 4. Results are summarized in Section 5, which is followed by the conclusion section.

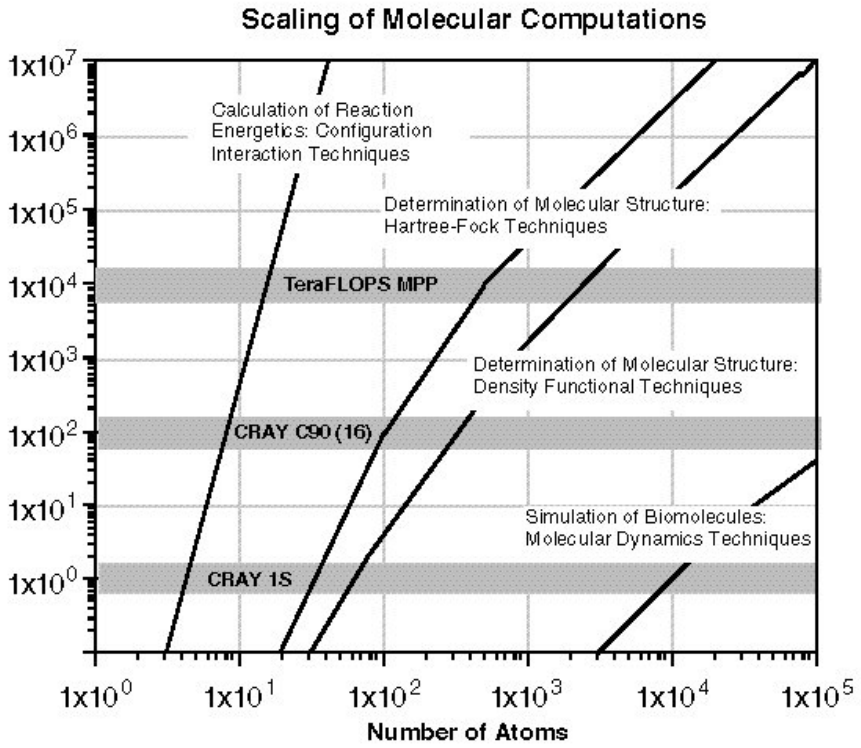

Figure 2: Computing time scaling as a function of the number of atoms for four methods

2 Nanoclusters

By definition, nanoparticles are particles of any shape with dimensions in the 1 to 100 nm range[4], while a nanocluster is a nanoparticle made up of equal subunits. These subunits can be atoms of a single element, molecules or even combinations of atoms of several elements in subunits with equal stoichiometry. The most extensively studied nanoclusters are metals and semiconductors, which can be either alloys or elemental substances.

2.1 Structure

The structure of nanoclusters can be a regular crystalline structure, amorphous, or form a pseudo close packing which cannot be classified by any of the crystallographic space groups. Each of these structures has a preferred set of numbers of the atoms involved in the cluster corresponding to optimum stable configurations, and this set is called the "magic numbers" in the literature. For instance, the sequence of magic numbers for the multiply twinned icosahedra are $N_m = 1, 13, 19, 43, 55, 79, 87, 135, 141, ...$[5]. The shape of nanoclusters is usually a polyhedron instead of a perfect sphere, as shown in Figure 3.

The magic numbers are determined by both electronic and structural favourites. Structural magic numbers are defined by the exact amount of atoms needed to build a certain potentially stable structure, which more frequently appear in large clusters, whereas in the case of small clusters the combined electronic structure of all of the atoms is of greater importance. One spherical quantum mechanical model called the "jellium model"[6] is especially suitable for describing the stability of alkali metal. The jellium model regards a cluster of atoms as a single large atom, where the distribution of ionic cores is replaced by a constant positive background, the so-called "jellium density", and only valence electrons are treated explicitly.

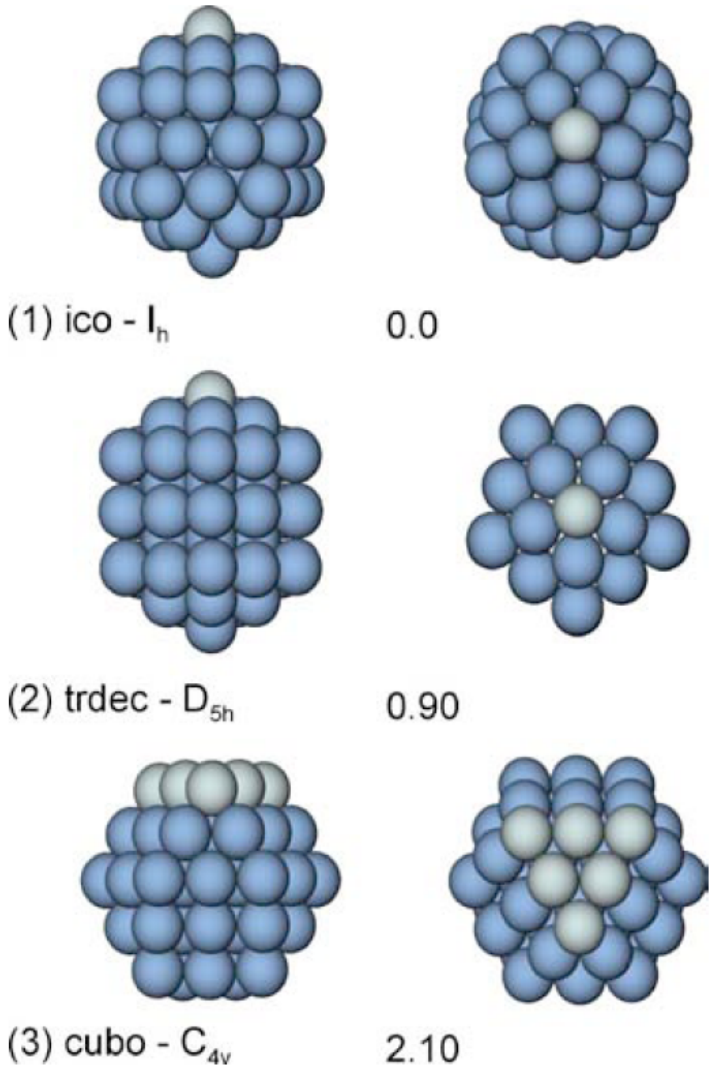

Figure 3: Isomers found for various Ag55 structures using DFT calculations. Shown are the optimized structures side-view left, top-view right together with point group symmetries and relative stabilities for Ag55[7]

2.2 Synthesis

In this section, only physical methods for synthesis of nanoclusters will be introduced, although there are many features in chemical and bio-chemical methods which are highly desirable for synthesizing nanoclusters, such as controllable sizes and compositions[8, 9]. Common synthesizing techniques within physical routine are ball milling[10], energetic vaporization[11, 12] and gas-phase condensation[4, 13]. Ball milling produces nanoparticles by mechanical attrition, producing grain size less than 5 nm. High-energy ball milling uses steel balls to transfer kinetic energy by impact to the sample. The major limitations are highly polydisperse products and contamination. Energetic vaporization use high-energy sources such as electric arcs, lasers, electron beams and plasmas(ion beams) to produce nanoparticles from bulk materials.

In this work, simulations are based on gas-phase condensation of silicon nanocluster. In gas-phase condensation system, as shown in Figure 4, the raw material is vaporized by magnetron sputtering and introduced into a flow of cold inert gas which has relatively high pressure. The vapour becomes highly supersaturated and starts to nucleate and grow into larger liquid nanoparticles. The size distribution of nanoclusters is controlled by several parameters such as sputtering rate, pressure in the chamber, gas flow rate, length of the drift region and size of aperture. The desirable features of gas-phase condensation process are (1) low contamination; (2) to produce large clusters and (3) a large fraction of the produced clusters is ionized. However, not all materials can be used in this technique.

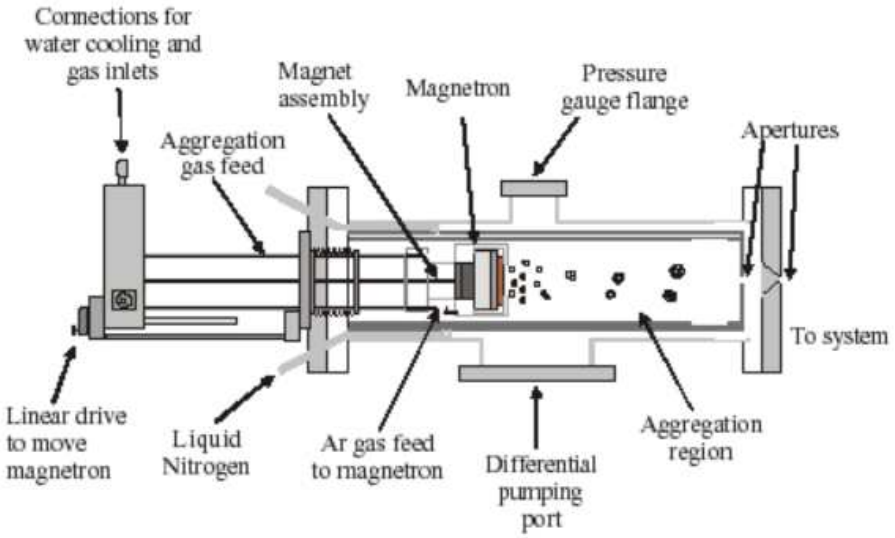

Figure 4: Nanocluster synthesis system for gas-phase condensation routine[14]

2.3 Properties

The abnormal properties of nanocluster appear due to two reasons: (1) quantum confinement in all three dimension; (2) large fraction of surface atoms. Quantum confinement can be understood as restriction of electrons in one or more dimension, which means that a continuum of electronic states in this dimension no longer exists[15]. Quantum confinement effect can be shown clearly by comparing the density of states for different dimensional materials, as shown in Figure 5. The density of states is a physical property of a material that indicates the structure and degree of packing of energy levels in a quantum mechanical system. In Figure 5, the density of states for bulk materials continually increases with energy; for 2D quantum well, it is like a stair case: it changes abruptly for larger changes but is continuous for smaller changes; the density of states for quantum wires is neatly discrete with some continuity; for quantum dots, it is very molecular-like in appearance with discrete peaks.

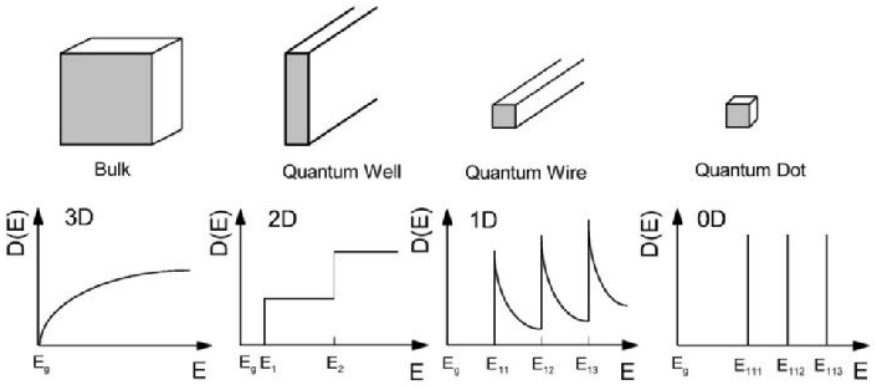

Figure 5: Electronic density of states for different dimensional materials[16]

The large fraction of surface atoms introduces extra surface energy in nanoclusters. In its simplest form, the surface energy E_s of a crystalline solid can be estimated as the number of surface atoms N_s times the one-half bonding energy per atom pair ε_b:

$$E_s = \frac{1}{2} N_s \varepsilon_b$$

In bulk materials, the fraction of surface atoms is so small that the effect of the surface can be neglected. In nanocluster, on contrary, the amount of surface atoms affect the properties drastically. For instance, the melting point dramaticly deviates from the bulk due to the high ratio surface atoms.

3 Metal-induced crystallization

Metal-induced crystallization(MIC) was first reported in 1972[17]. It is a method turning amorphous silicon(a-Si) into polycrystalline at relatively low temperature by direct contact with a metal layer. It has been investigated extensively as an alternative crystallization process in silicon based photovoltaic industry. In this section, experimental and theoretical studies of this process in macro-scale system are reviewed.

3.1 Crystallization process

Crystallization is a phase transformation process by which, upon cooling, an ordered solid phase is produced from a solution, melt or amorphous solid phase[18]. The progress of crystallization may be broken down into two distinct stages: nucleation and growth. Nucleation involves the appearance of very small crystallized nuclei, which can be either homogeneous or heterogeneous. For the homogeneous type, nuclei of crystallization form uniformly throughout the liquid phase, whereas for the heterogeneous type, nuclei form preferentially at structural inhomogeneities, such as surface, insoluble impurities, grain boundaries and dislocations. For the homogeneous type, the critical nucleus radius r^* can be calculated by knowing the surface free energy γ and the difference between two phases ΔG_v :

$$r^* = -\frac{2\gamma}{\Delta G_v}$$

and the activation free energy required for the formation of a stable homogeneous nucleus ΔG^*_{hom} is:

$$\Delta G^*_{hom} = \frac{16\pi\gamma^3}{3(\Delta G_v)^2}$$

For the heterogeneous type, the critical raduis r^* is the same as for homogeneous, but the activation energy barrier is smaller than the homogeneous barrier by an amount corresponding to the value of the function $S(\theta)$:

$$\Delta G^*_{het} = \Delta G^*_{hom} S(\theta)$$

where $S(\theta)$ is a function only of the shape of the nucleus, which will have a numerical value between zero and one. A schematic graph (Figure 6) plots curves for both types of nucleation and indicates the difference in the magnitudes of ΔG^*_{het} and ΔG^*_{hom}, in addition to the constant value r^*. This lower ΔG^* for heterogeneous nuclei means that a smaller amount of energy must be overcome during the crystallization process, therefore, heteroge-

neous nucleation occurs more frequently. This conclusion is the motivation for us to study metal-induced crystallization.

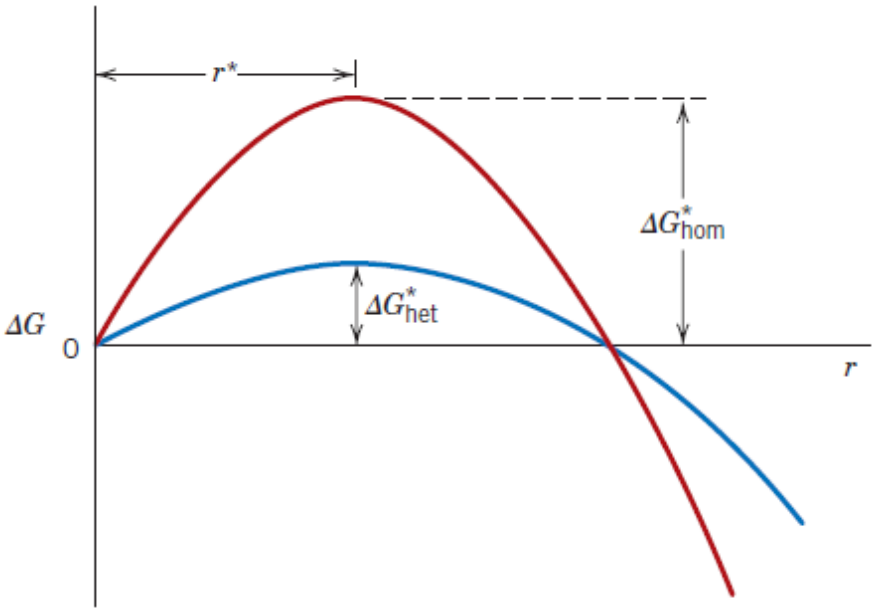

Figure 6: Schematic graph of ΔG versus nucleus radius, plots curves for both types of nucleation[18]

3.2 Experimental study

In 1972, MIC process was first discovered by material scientists in IBM research center. At that time, they found out that silicon crystallized at 0.72 (0.65 for germanium) of the eutectic temperature. The MIC process involves the deposition of a-Si films on top of which a layer of suitable metal is deposited. This bilayer of metal and Si is then annealed in a furnace at temperature ranging from 400 K to 1000 K for durations between one minute and several hours leading to crystallization of the a-Si. In 1994, T. J. Konno and R. Sinclair[19] used transmission electron microscopy to investigate the Ag/a-Si system and proposed layer exchange mechanism. Figure 7 shows a schematic illustration of such a layer exchange process based on model proposed by Nast and Wenham[20, 21]. A bilayer structure of a catalyst (metal) and a-Si is deposited on a glass substrate. Silicon atoms diffuse from the a-Si layer to the metal layer during the annealing process. The diffusion is a nonequilibrium process and leads to supersaturation of the metal layer with silicon atoms. This supersaturation will lead to the formation of crystalline silicon (c-Si) nuclei in the metal layer. The c-Si nuclei continuously grow until they reach the substrate interface or other c-Si phase.

The whole process finishes until the layers have completely changed their relative positions. The initial interaction of the catalyst (metal) and a-Si layers involves the partial dissolution of the metal or silicon oxide interface layer, It is believed that this thin diffusion barrier between the catalyst and the silicon is important for the layer exchange, which prevents uncontrolled and random intermixing of two layers.

Until now, Al[22], Au[23], Ag[24], Sn[25], Cr[26] and Ni[27, 28] have been applied in MIC process. These metals are classified in two groups based on the mechanism how they crystallize the amorphous Si. Au, Ag, Al and Sn[29] form eutectic alloy with a-Si matrix and Cr and Ni forms silicide with Si. The lowest limit for the crystallization temperature is 420 K when a-Si is in contact with Al[22, 30]. However, the equilibrium solubility of aluminium in silicon is still relatively large (up to 1.5 at. percent)[29], aluminium-induced crystallization should lead to highly p-doped films. This undesirable feature can be overcome by using silver which has negligible solubility in silicon. The reported crystallization temperature of Ag/a-Si system is about 620 K[24], which enables the use of quartz and glass substrate, since the melting points of quartz and glass are about 1700-1900 K[31].

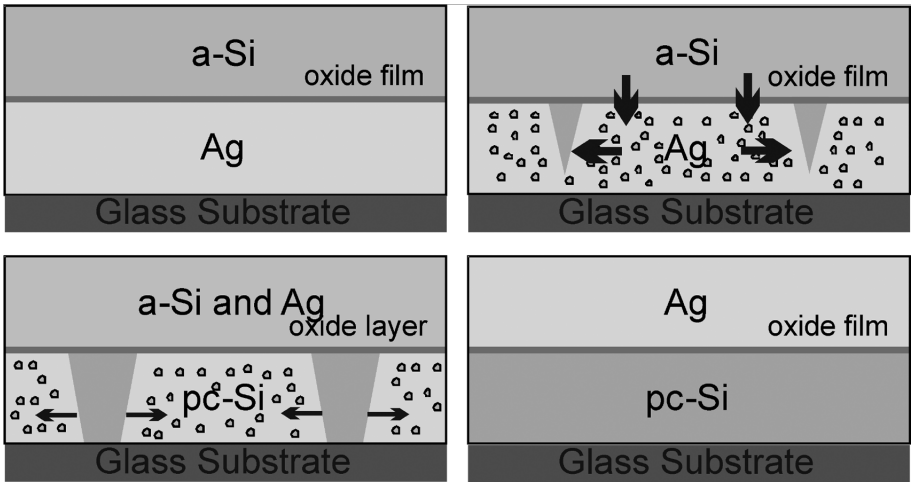

Figure 7: Schematic view of the metal-induced layer exchange process based on the model proposed by Nast and Wenham[20]

3.3 Theoretical models and mechanisms

According to the general "screening model" suggested by Hiraki[32], the covalent bonds in amorphous silicon become weakened at the interface with a metal layer, allowing for a relatively high mobility of the interfacial atoms, which may provide the agent for initiation of crystallization of amorphous silicon at relatively low temperature. This bond-weakening

effect is a very local electronic interaction phenomenon, and the effected interfacial silicon atoms has been estimated to be within about two monolayers[33].

These two monolayers of interfacial silicon atoms in a-Si could lower the Gibbs energies of the system by (a) crystallizing, (b) dissolving into the metal layer, (c) reacting with the metal to form a silicide, or (d) diffusing to grain boundaries in the metal. Which process can occur depends on the competition between the change of bulk Gibbs energies and the change of corresponding surface and interface energies.[22] As an example, the critical thickness for nucleation of c-Si at the Ag/a-Si interface as a function of temperature T, can be calculated by dividing the increase of interface energy corresponding to crystallization by the decrease of the "bulk" Gibbs energy:

$$l^{critical}_{Ag/a-Si}(T) = \frac{\gamma^{interface}_{\langle Si\rangle/\langle Ag\rangle}(T) + \gamma^{interface}_{\langle Si\rangle/\{Si\}}(T) - \gamma^{interface}_{\{Si\}/\langle Ag\rangle}(T)}{-\Delta G^{crystallization}_{\langle Si\rangle-\{Si\}}(T)}$$

where the braces $\{\}$ and brackets $\langle\rangle$ denote the amorphous and crystalline phases respectively, so, for instance, the term $\gamma^{interface}_{\{Si\}/\langle Ag\rangle}(T)$ means the interface energy (in J/m^2) between a-Si and crystallized silver as a function of temperature T, and the term $-\Delta G^{crystallization}_{\langle Si\rangle-\{Si\}}(T)$ is the bulk crystallization energy (in J/m^3). In order to have the stable nucleation at the Ag/a-Si interface at a given temperature, the critical thickness for nucleation should be smaller than or equal to two monolayers. In the reference, the calculated critical thickness is 2.7 monolayers at Ag/Si interface. This indicates that the nucleation of crystallization is undesirable to occur at the interface but exclusively proceed at Ag grain boundaries.

4 Retrograde Melting

Retrograde melting[34] is known as a high-temperature phase transition of metal impurities in silicon, where the processing conditions force metal impurity atoms to cluster and precipitate out of solution into liquid metal-silicon droplets within the larger, solid silicon crystal. Simply speaking, it is a phenomenon where a liquid second phase decomposes from a solid solution upon cooling[35]:

$$Solid \longrightarrow Solid + Liquid$$

Retrograde melting is related to retrograde solubility[36], where the maximum concentration of metal atoms in silicon solution occurs at a temperature higher than the eutectic temperature (the lowest temperature at which liquid can exist in the binary system). It is not the case in many metallic systems, where the maximum solubility occurs at the eutectic temperature. A schematic example of retrograde melting is shown in Figure 8. When cooling a silicon solution with highly concentrated metal impurity at the temperature above the eutectic temperature of the system, because the slope of the retrograde solvus line is negative, the solution will become supersaturated. Precipitation will occur when the chemical potential driving force led by the supersaturation is greater than the nucleation energy barrier for precipitation. Because the supersaturated system exists at temperatures higher then the eutectic temperature, precipitates will form in the liquid phase causing retrograde melting, where local melting occurs upon cooling. This driving force due to supersaturation can be described as a reduction in bulk free energy per atom achieved by the precipitation of a second phase[37]:

$$\Delta f = k_B T ln \frac{c_M}{c_M^{eq}}$$

where Δf is the reduction in free energy per metal atom, c_M^{eq} is the equilibrium solubility at the system temperature, c_M is the actual concentration of dissolved metal. In this way, the maximum driving force for retrograde melting in a given binary system can be derived if the system starts from the temperature of maximum solubility and cooled to the eutectic temperature without precipitation:

$$\Delta f_{max} = k_B T_{eut} ln \frac{c_M(T_{max})}{c_M(T_{eut})}$$

where T_{eut} is the eutectic temperature and T_{max} is the temperature of maximum solid solubility.

In the case of silver-silicon(Ag-Si) system, an equilibrium phase diagram is shown in Figure

9. The system has eutectic reaction around 1108K and 89 atomic percent Ag. The mutual solubility of Si and Ag in the solid state are negligible. However, as shown in Figure 10, it is also reported that the solid solubility of Ag in Si in high-temperature range is retrograde in character with the maximum solid solubility $c_{Ag}(T_{max}) = 6.5 \times 10^{16}/cm^3$ at about 1620 K and the extrapolated solid solubility $c_{Ag}(T_{eut}) = 1.8 \times 10^{6}/cm^3$ (extrapolated from available experimental data at lower temperature)[36]. Therefore, the calculated maximum driving force is $\Delta f_{max} = 2320 meV/atom$. These data gave us the inspiration that Ag-Si binary system is possible to have retrograde melting process.

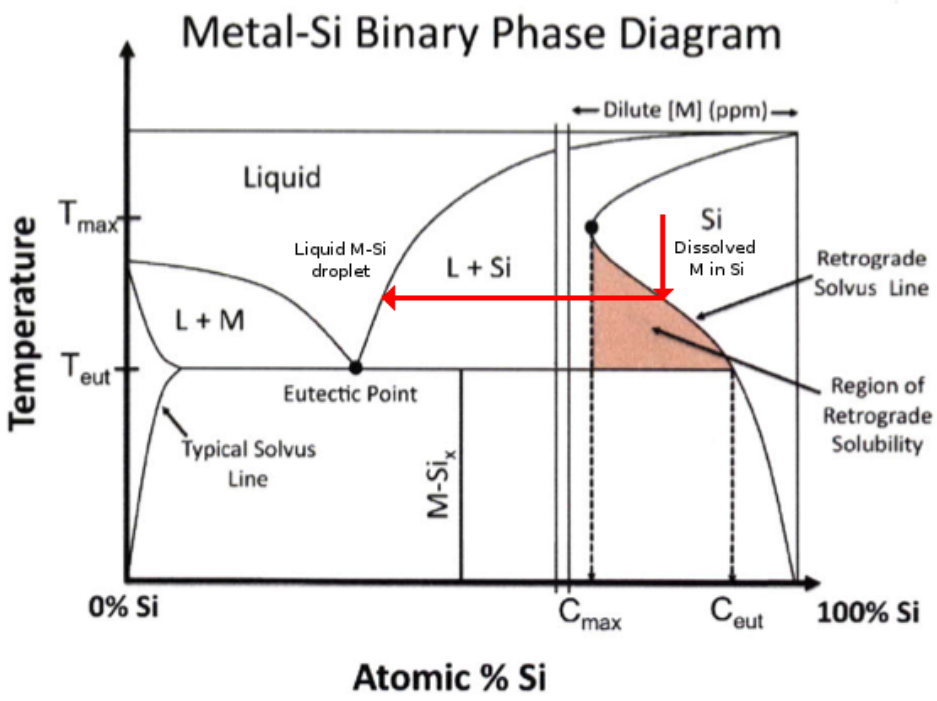

Figure 8: A schematic binary phase diagram shows how retrograde solubility of a dissolved metal (M) in silicon can lead to retrograde melting upon supersaturation above the eutectic temperature, forming liquid M-Si droplets.

Recently, experimental researchers in Okinawa, Japan have shown a nanoscale version of this process involving undercooled liquid Si nanoparticles inoculated with silver nanoclusters. Undercooled Si nanoparticles were produced by using a gas aggregated magnetron sputtering system. In the experiment, a supersaturated Si vapour was generated by DC magnetron sputtering of a high purity Si target mounted in a water cooled aggregation chamber(Figure11 part 1, labelled 'I'). Nucleation of liquid Si clusters occurs in Ar gas atmosphere at relatively high pressure, and is followed by the nucleation and growth of larger liquid Si nanoparticles due to coalescence. Due to the pressure difference between the aggregation zone and the sample deposition zone(Figure11 part 1, labelled 'III'), the

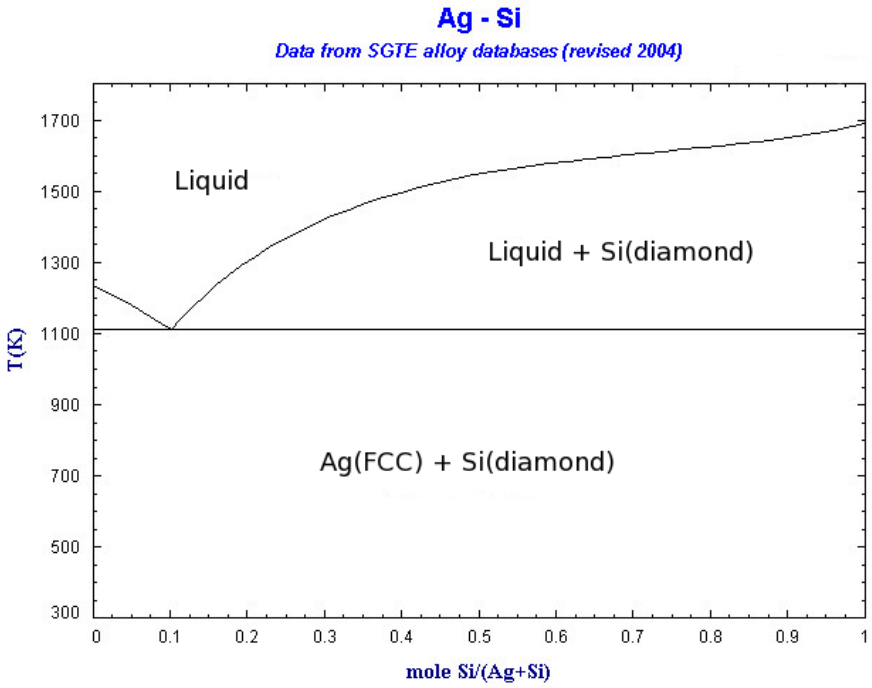

Figure 9: Si-Ag phase diagram from SGTE alloy database[38]

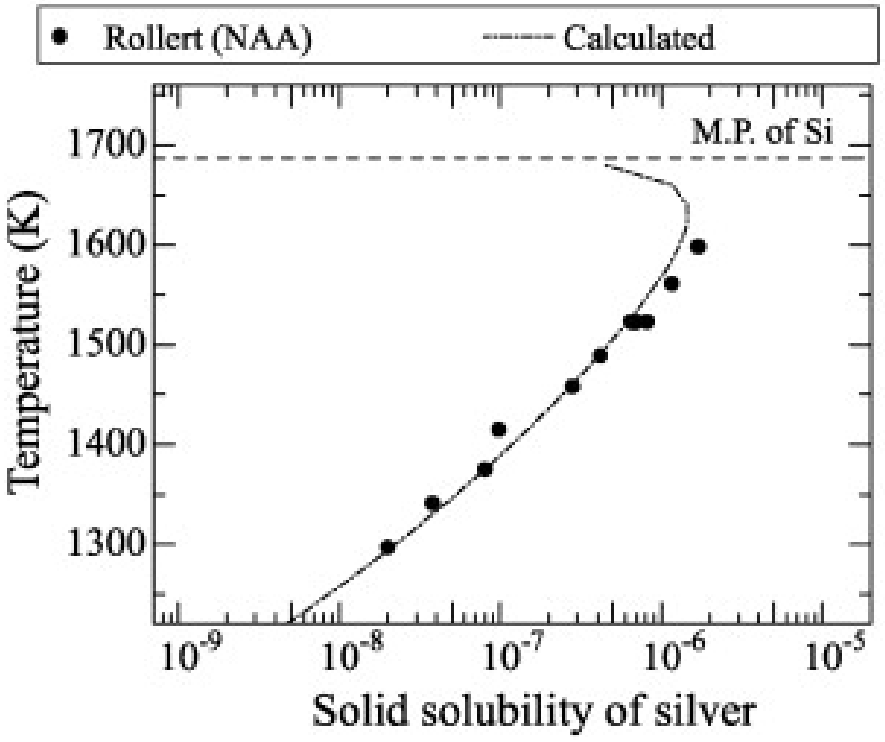

Figure 10: Solid solubility of Ag in Si[39]

nucleated liquid Si nanoparticles is transported through the differential pumping orifice and out of the aggregation zone. In the inoculation zone(Figure11 part 1, labelled 'II'), silver atoms sputtered from a linear magnetron sputtering target are inoculated in the liquid Si nanoparticle. Finally, the inoculated Si nanoparticle deposited on substrates. Figure11 part 2 shows that Ag inoculated Si nanoparticles were nanocrystallized under the presence of the Ag nanoclusters. There is a direct correlation between the number of Ag nanoclusters and the number of nanograins in the Si core.

What the actual mechanism of crystallization of Si nanoparticles is still remains a question. This nanocrystallization process can be interpreted in two ways: Metal-induced Crystallization(MIC) or retrograde melting, based on whether the temperature of the Si nanocluster during the crystallization is high enough to remelt the cluster. In order to reveal the mechanism, molecular dynamics simulations were carried out to reproduce the Ag condensation on liquid Si nanoparticles.

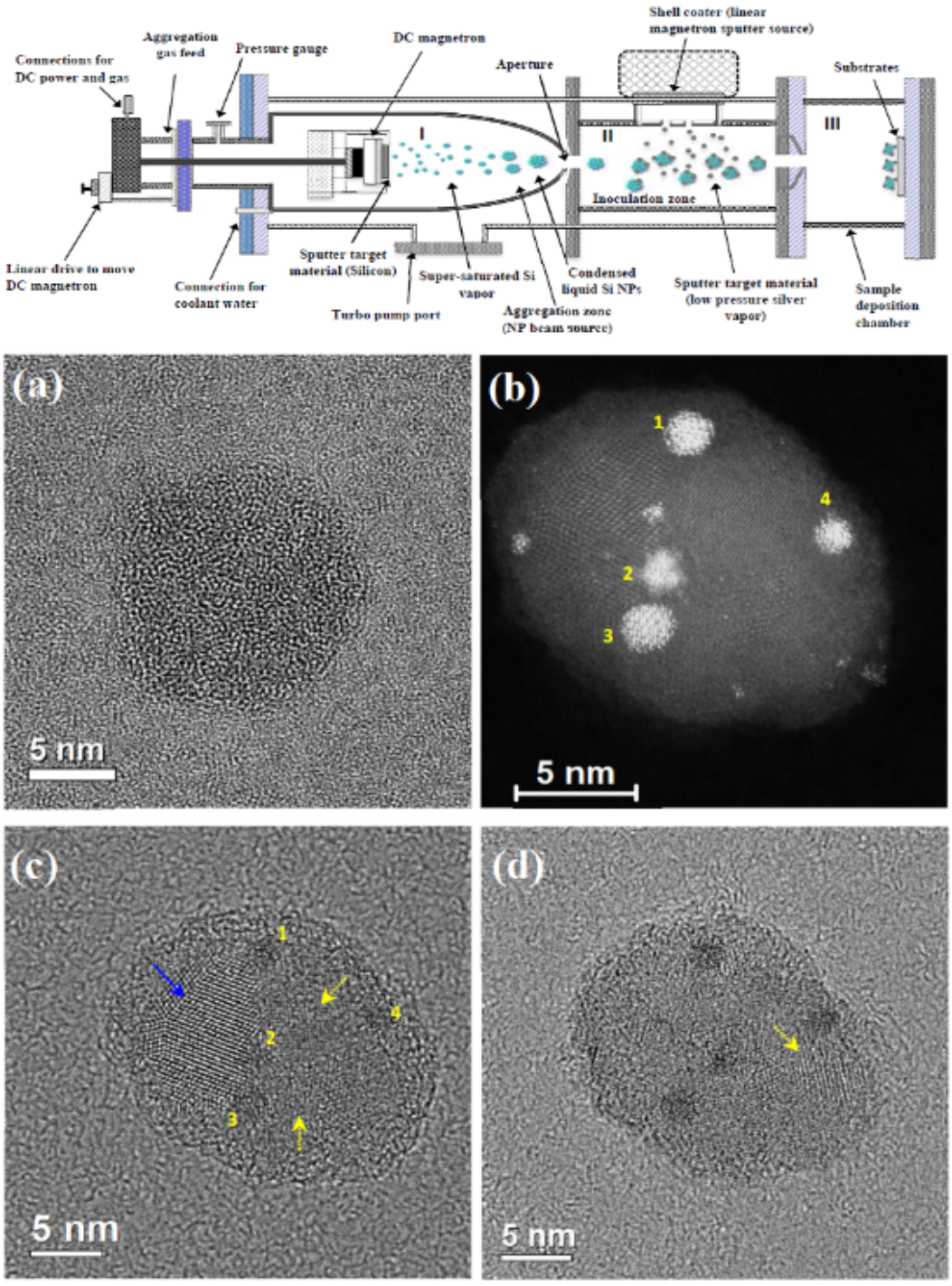

Figure 11: 1. Schematic drawing of the magnetron sputter inert gas condensation setup used to produce Ag nanocluster-inoculated Si nanoparticles. 2. HAADF-STEM and HRTEM images of the Si nanoparticles: (a) TEM image of an amorphous Si nanoparticles without the presence of Ag inoculation. (b) HAADF-STEM image of Si nanoparticle inoculated with several Ag nanoclusters marked by numbers 1-4. (c)(d) TEM images of the same nanoparticle. Arrows indicate the crystallized regions.[40]

5 Methods

5.1 Molecular dynamics

5.1.1 Algorithm

Molecular dynamics (MD) is a computer simulation method of physical movements of atoms and molecules, whose trajectories are determined by numerically solving Newton's equations of motion for a system of interacting particles. Based on the ergodic hypothesis that the statistical ensemble averages are equal to the time averages of a system, the results of MD simulations can be used to determine the macroscopic thermodynamic properties of the system. MD methods couple the microscopic length and time scale and the macroscopic world of the laboratory: a model is made to describe the interactions between atoms, and predictions of bulk properties are obtained. MD simulations provide great insights into qualitative mechanisms of radiation effects, which facilitates the interpretation of the experimental results.

The general description of the basic MD algorithm is shown in Figure 12. Computing the interatomic forces in an MD simulation involves a large number of pairwise calculations, normally carrying out N^2 operations for each time step in an N-atom system. For most cases, the atomic interaction potentials can be limited within a certain range r_{cut} from each atom, $V(r_{ij}) = 0$ if $r_{ij} > r_{cut}$. This range r_{cut} is denoted by a cut-off distance. To avoid the N^2 operations not only when calculating the inter-atomic potential, but also when checking whether $r_{ij} \leq r_{cut}$ for atoms i and j, we can generate a neighbour list for each atom. A method to speed up a program was suggested by Loup Verlet by constructing of all the neighbours of each atom within a new distance r_{list} ($r_{list} > r_{cut}$) [41]. Over the next few time steps, only pairs in the list are checked in the force routine. The list should be updated every N_m steps to avoid unlisted pairs coming within the interaction range. Verlet neighbour list is probably the easiest efficient way of constructing a neighbour list. However, for larger systems, the cell index method [42, 43], an advanced way to reduce the complexity from N^2 to N, becomes preferable.

The atomic forces are calculated by the potential energy function $U(r^N)$:

$$\boldsymbol{f_i} = -\frac{\partial}{\partial r_i} U(\boldsymbol{r^N})$$

For a pure pair potential, $U_{ij} = U_{ji}$, where U_{ij} is the pair potential with two-body terms $U_{ij} = U_2(\boldsymbol{r_i}, \boldsymbol{r_j})$. Since the potential only depends on r_{ij}, this is a simple calculation: the

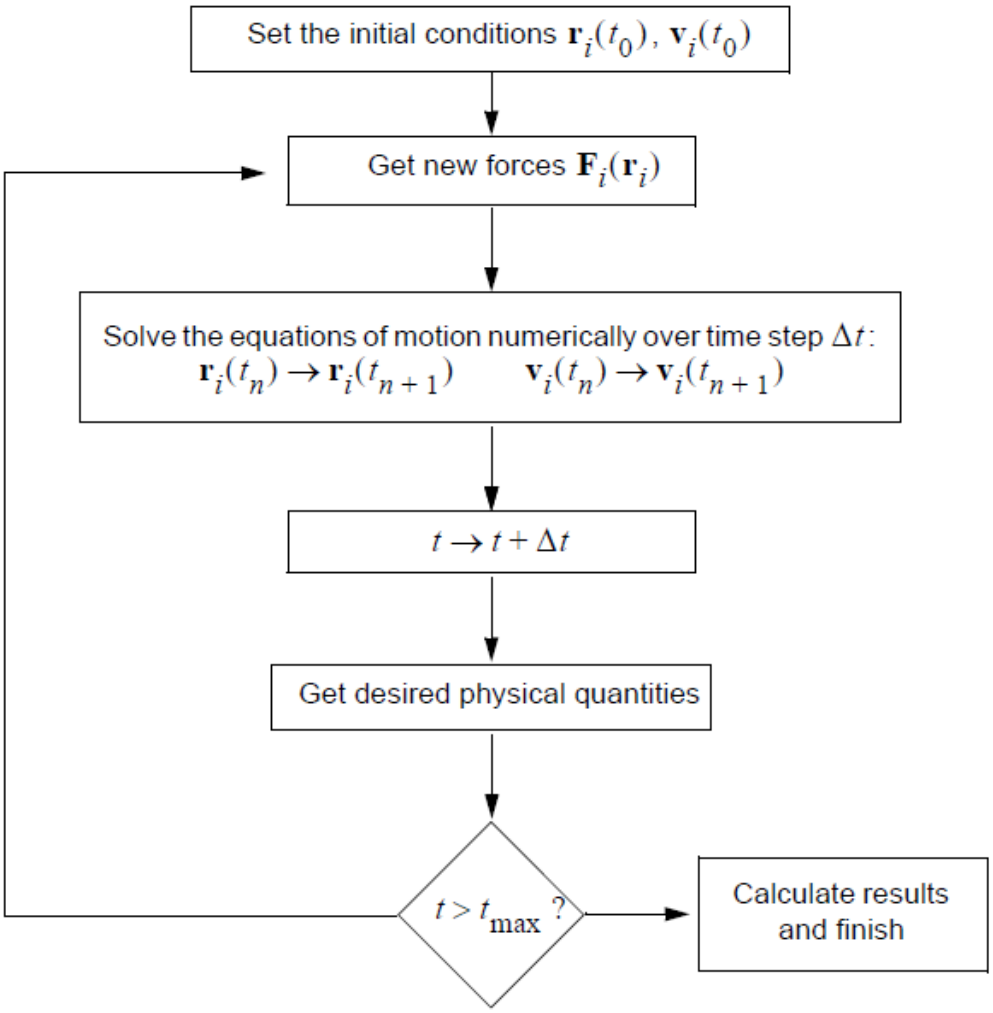

Figure 12: Description of the basic MD simulations algorithm.

force acting on atom i due to atom j is

$$\boldsymbol{f_{ij}} = -\nabla_{r_{ij}} U_2(r_{ij}) = +\nabla_{r_{ji}} U_2(r_{ij}) = -\boldsymbol{f_{ji}}$$

However, in the case of a three-body potential, things are more difficult since $U_{ij} \neq U_{ji}$. Now we have both two-body terms $U_{ij} = U_2(\boldsymbol{r_i}, \boldsymbol{r_j})$ and three-body terms $U_{ijk} = U_3(\boldsymbol{r_i}, \boldsymbol{r_j}, \boldsymbol{r_k})$. The force now becomes:

$$\boldsymbol{f_i} = -\nabla_i [\sum_j (U_{ij} + U_{ji}) + \sum_{j,k} U_{ijk}],$$

where $\boldsymbol{r_i}, \boldsymbol{r_j}, \boldsymbol{r_k}$ are the position vectors of three interacting atoms in the system. More details of how to do it are given in appendix C of Ref. [44].

The simulation proceeds iteratively by alternatively calculating forces and solving the equations of motion based on the accelerations obtained from the new forces. The Verlet algorithm tends to be favoured to numerically solve equations of motion. There are various versions of the Verlet algorithm, including the standard method [41, 45], and a 'leapfrog' form [42]. Here we introduce the 'velocity Verlet' algorithm [46] since its numerical stability, convenience and simplicity make it a very attractive candidate for MD codes. Velocity Verlet can be implemented in a two-step predictor-corrector algorithm with a predictor step:

$$r(t + \Delta t) = r(t) + \Delta t v(t) + \frac{1}{2}\Delta t^2 a(t)$$

$$v^p(t + \frac{1}{2}\Delta t) = v(t) + \frac{1}{2}\Delta t a(t)$$

and a corrector step:

$$v^c(t + \Delta t) = v^p(t + \frac{1}{2}\Delta t) + \frac{1}{2}\Delta t a(t + \Delta t),$$

where v is the velocity, and a is the acceleration.

5.1.2 Temperature control

The algorithms used to integrate the equations of motion conserve the total energy of system (if they are correctly implemented). In many circumstances, the explicitly simulated system is assumed to be just a small part of a macroscopic system which acts as a thermostat. This corresponds to a canonical ensemble, where particle number(N), volume(V) and temperature(T) are fixed, and the total energy(E) may change. Also in equilibrium, the Helmholtz free energy, $F = U - TS$, is minimized. The heat exchange with the heat bath is modelled by a thermostat acting on the atomic velocities. If simple scaling is needed, the Berendsen thermostat[47], simply rescaling the velocities of the atoms in the system to control the simulation temperature, is applied. The system temperature will relax exponentially to the desired temperature T_0 with a time constant τ:

$$\frac{dT}{dt} = \frac{T_0 - T}{\tau}$$

The Berendsen method is simple and efficient but it does not sample the canonical ensemble. Therefore, this method is only good for the initial system setup and equilibration. For accurate temperature control or canonical ensemble thermodynamic averaging, Nosé-Hoover thermostat[48, 49] is used. The equations of motion are modified by a temperature

dependent friction parameter ξ:

$$\frac{d^2\mathbf{r}_i}{dt^2} = \frac{\mathbf{f}_i}{m_i} - \xi\frac{d\mathbf{r}_i}{dt}$$

following the equation of motion:

$$\frac{d\xi}{dt} = \frac{T - T_0}{Q}$$

where $\mathbf{r}_i$ and m_i are the position and mass of particle i, and $\mathbf{f}_i$ is the force acting on particle i. Using this approach, the temperature will relax by a damped oscillation towards the desired temperature and the coupling strength is determined by the mass parameter Q. The coupling is described by the time constant τ of the kinetic energy fluctuations, which is directly related to Q and T_0:

$$\tau = 2\pi\sqrt{\frac{Q}{T_0}}$$

5.1.3 Pressure control

Similar to specifying temperature in MD simulation, it may be desirable to maintain the system at constant pressure and let the volume V of the simulation box fluctuate. The Berendsen barostat[50] is analogous to the Berendsen thermostat. The box-center-of mass coordinates are scaled at each MD step:

$$\mathbf{r}' = X^{1/3}\mathbf{r}$$

$$X = 1 - \kappa\frac{\Delta t}{\tau_P}(P - P^{(int)}(t))$$

where $\kappa = -\frac{1}{V}(\frac{\partial V}{\partial P})_T$ is isothermal compressibility, and τ_P is relaxation time for the coupling. The Berendsen method drives the system pressure according to equation:

$$\frac{dP^{(int)}(t)}{dt} = \frac{1}{\tau_P}(P - P^{(int)}(t))$$

As the Berendsen thermostat, the barostat is exponentially damped and drives the system to the desired pressure. An other widely used method is the Parrinello-Rahman barostat. In the extended-ensemble[51, 52], the matrix of simulation box vectors b follows an equation of motion:

$$\frac{d^2b}{dt^2} = V\mathbf{W}^{-1}b^{T-1}(\mathbf{P} - \mathbf{P}_0)$$

where V denotes the box volume, $\mathbf{W}^{-1}$ is the coupling strength, and $\mathbf{P}$ and $\mathbf{P}_0$ are the instantaneous and target pressure tensors, respectively. The equations of motion of the atoms are modified by:

$$\frac{d^2\mathbf{r}_i}{dt^2} = \frac{\mathbf{f}_i}{m_i} - M\frac{d\mathbf{r}_i}{dt}$$

with

$$M = b^{-1}[b\frac{d\mathbf{b}^T}{dt} + \frac{d\mathbf{b}}{dt}\mathbf{b}^T]\mathbf{b}^{T-1}$$

5.1.4 Interaction potentials

In the following, we will briefly discuss the potential used in this work.

The Lennard-Jones (LJ) potential [53] is the most commonly used form, developed from the study of inert gas. In this work, the LJ potential is applied for Ar-Ag and Ar-Si interaction. One special feature is that there is no interaction between Ar and Ar atoms. The potential is:

$$V_{LJ}(r) = 4\varepsilon[(\frac{\sigma}{r})^{12} - (\frac{\sigma}{r})^{6}]$$

where σ represents the atomic diameter and ε measures the strength of the interaction. For argon, the values of ε and σ are $\varepsilon = 1.65 \times 10^{-21}J$ and $\sigma = 3.4 \times 10^{-10}m$[54]. LJ potential works reasonably well for noble gases close to equilibrium. However, due to $V(r) \propto r^{-12}$, it fails badly at very close interatomic separations (the true behaviour is $V_r \propto e^{-r}/r$).

The potential applied for Si-Si interaction is proposed by Stillinger and Weber[55]. This empirical potential model contains both two- and three-body interactions in order to reflect the directional characteristics of the covalent bonding.

$$V = \sum_{i<j} V_2(r_{ij}) + \sum_{i<j<k} V_3(r_i, r_j, r_k)$$

The two-body part models the bonds:

$$V_2(r) = \begin{cases} A(Br^{-p} - r^{-q})exp[(r-a)^{-1}] & r < a \\ 0 & r \geq a \end{cases}$$

and the three-body term is given by:

$$V_3(r_i, r_j, r_k) = h(r_{ij}, r_{ik}, \theta_{\widehat{jik}}) + h(r_{ji}, r_{jk}, \theta_{\widehat{ijk}}) + h(r_{ki}, r_{kj}, \theta_{\widehat{ikj}})$$

where

$$h(r_{ij}, r_{ik}, \theta_{\widehat{jik}}) = \begin{cases} \lambda exp[\gamma(r_{ij} - a)^{-1} + \gamma(r_{ik} - a)^{-1}] \times (cos(\theta_{ijk}) + \frac{1}{3})^2 & r_{ij} < a \\ 0 & otherwise \end{cases}$$

where r is the distance between a pair of atoms, r_{ij} is given by $r_{ij} = |r_i - r_j|$, and $\theta_{\widehat{jik}}$ is the angle subtended by r_{ij} and r_{ik} with the vertex at the ith site. The constants A, B, p, q, a, λ and γ are all positive and are taken for the case of the most stable diamond structure. The parameters are presented in Table 1:

A	B	p	q	a	λ	γ
7.04955628	0.60222456	4	0	1.80	21.0	1.20

Table 1: Parameters used in Stillinger-Weber potential for silicon

Embedded atom method (EAM) potential proposed by Foiles et. al.[56], is applied for the Ag-Ag interaction. The EAM represent the total energy of an atomic system in the form:

$$E_{tot} = \frac{1}{2} \sum_{ij} V_{ij}(r_{ij}) + \sum_{i} F_i(\overline{\rho}_i)$$

where $V_{ij}(r_{ij})$ is the pair interaction energy between atoms i and j separated by a distance r_{ij} and F_i is the embedding energy of atoms i as a function of the host electron density $\overline{\rho}_i$. The latter is given by:

$$\overline{\rho}_i = \sum_{j \neq i} \varphi_j(r_{ij})$$

This model only accounts for two atoms interaction and not for more complex structure.

For Ag-Si mixed interaction, the pair potential is determined from a gas phase dimer calculated with a density functional theory approach. Since a potential for a gas phase dimer is known to overestimate the bond energy in the bulk, the obtained Ag-Si dimer potential was rescaled in the attractive part to provide an interaction that causes Ag and Si in the bulk to mix in the liquid phase, but segregate in the solid phase, as expected from the phase diagram. This behaviour of the potential was checked with test simulations of initially liquid Ag and Si in a condensed system with periodic boundaries.

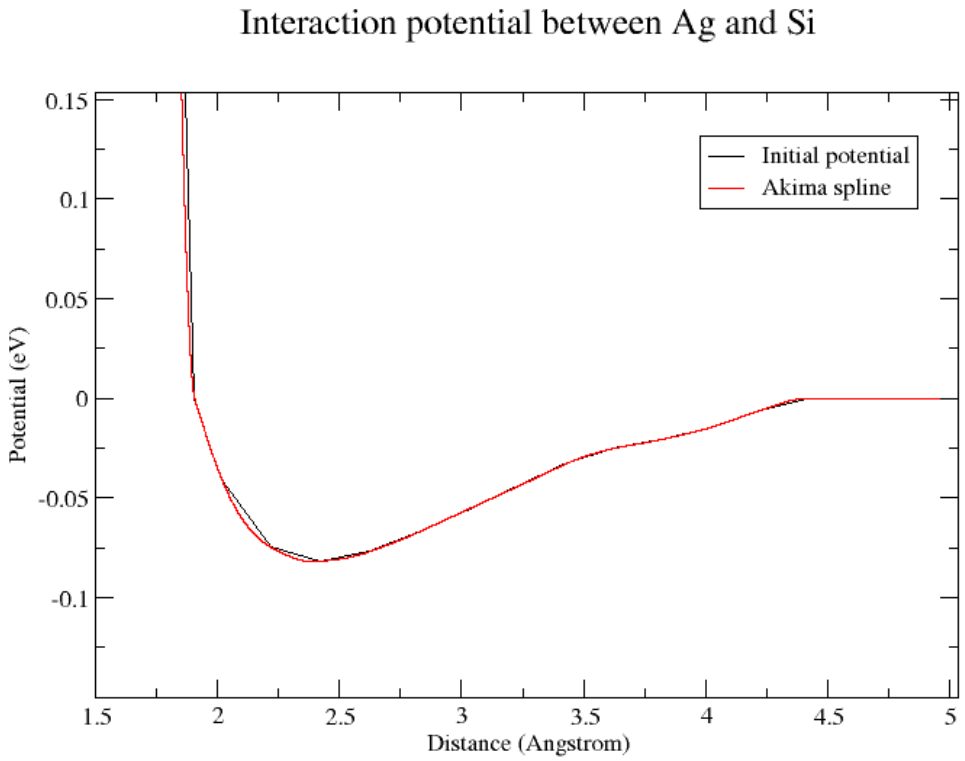

Figure 13: Ag-Si mixed interaction

5.2 Simulations of silver-induced crystallization in silicon nanoclusters

In this work, we set up the molecular dynamics simulation to imitate the conditions in the Ag inoculation zone in the experimental setup in Figure 11. A pure Si nanocluster which consists of 1677 atoms was located at the center of the simulation cell. The surrounding atmosphere contained Ar and Ag atoms, the former were fixed at 1000 atoms for all the cases and the latter amounted to various numbers from 67 to 400. All the silver and argon atoms are initially isolated, evenly filling the simulation cell, as shown in Figure 17(a). The initial velocities of all atoms were determined by using normally distributed random numbers to ensure a certain initial temperature in all simulations. For each specific combination of Si, Ag and Ar atoms, the initial temperature of Si atoms was altered from 1700 K up to 4000 K which ensured that the initial state of Si nanocluster was the liquid phase without evaporation and the initial temperature of Ag atoms was set to 1000 K, 2000 K and 3000 K to gain understanding of the dependence of the results on the temperature of Ag atoms. Besides, the temperature of Ar atoms was constantly set to 300 K($\pm$ 10 K) thus the temperature of

whole system was reduced via the thermal bath of the Ar atmosphere. The simulation cell was a cube of 400 nm side length with periodic boundary conditions. The total simulation time was 100 ns in all cases.

The internal MD unit system used in PARCAS is established in the way of minimizing the number of multiplications in the solution of the equations of motion. Here the units for a quantity in SI units are signed with$\widehat{\ }$. The MD energy $\widehat{E}$ is electron volts ($1eV = 1.6022 \times 10^{-19}J$), and the MD length unit is Angstrom ($1Angstrom = 10^{-10}m$). The crucial feature is that all atoms, regardless of their true mass, have a mass $\equiv 1$ in the MD unit system, therefore, many basic mechanics equations get a simple form, such as kinetic energy:

$$E = \frac{1}{2}v^2$$

Based on this we can derive the unit of v, which will depend on the mass m_i,

$$\widehat{v_i} = \sqrt{\frac{\widehat{E}}{m_i}}\frac{m}{s}$$

which also can be written,

$$\widehat{v_i} = \sqrt{\frac{e}{m_i(u)u}} = \frac{9822.66}{\sqrt{m_i(u)}}\frac{m}{s}$$

The maximum length of the time step unit $\widehat{t_i}$ in PARCAS code is determined from the atom type actually present in the system which has the lowest mass in this case it is silicon:

$$\widehat{t_{Si}} = \frac{\widehat{r}}{\widehat{v_{Si}}}s = 10.1805 * \sqrt{m_{Si}(u)}fs = 53.95fs$$

therefore, when $\Delta = 0.02$, the maximum time step is $1.079fs$.

5.3 Analysis of fraction of amorphous atoms

To quantify the degree of amorphization in a nanosystem, an angular structure factor P_{st} [57]is calculated for each atoms i:

$$P_{st}(i) = \frac{1}{p_u(i)}\{\sum_j(\theta_i(j) - \theta_i^p(j))^2\}^{1/2}$$

$$p_u(i) = \{\sum_j(\theta_i^u(j) - \theta_i^p(j))^2\}^{1/2}$$

where $\theta_i(j)$ is a list of the angles formed between atom i and its neighbours j. The number of the neighbours is determined from the ideal crystal structure, which for the diamond structure (Si) is 4 and for the FCC structure is 12. $\theta_i^p(j)$ is the distribution of angles in a perfect lattice and $\theta_i^u(j) = j\pi/[n_{nb}(n_{nb}-1)/2]$ the uniform angular distribution. Before doing the sum over angles the $\theta_i(j)$ lists are sorted by magnitude. By averaging the structure factor of each atom, combined with a kinetic energy criterion, we can analyse the degree of amorphization as a function of simulation time.

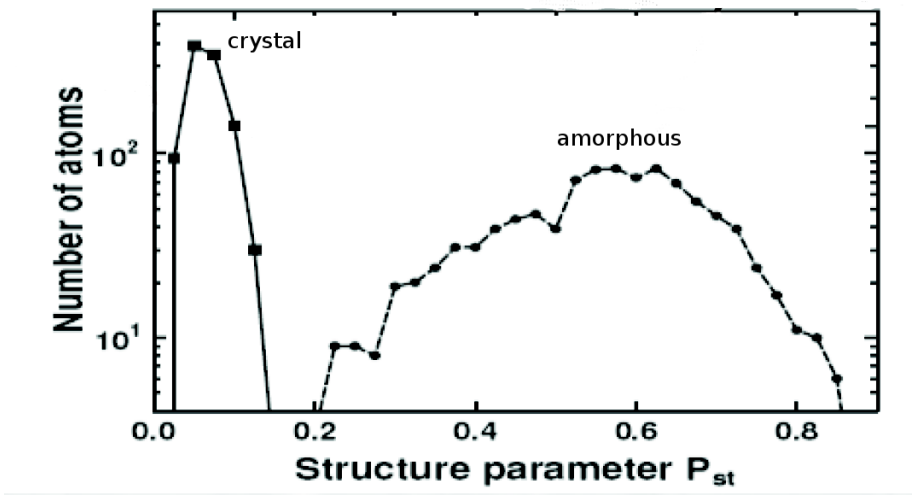

Figure 14: Distribution of the structure parameter P_{st} for crystallized and amorphous structure.[57]

6 Results and discussion

6.1 Results

In this work, molecular dynamics simulation was used to reproduce the silver induced crystallization process. The evolution of the temperature and the fraction of the amorphous atoms in the Si nanocluster was analysed to reveal the mechanism of crystallization of Si nanoparticles.

6.1.1 Undercooling of silicon nanocluster

As the beginning of the project, we carried out simulations to determine the melting temperature of pure silicon nanocluster with different diameters and the undercooling processes. These data will be used as a reference which help us to determine whether the maximum temperature reached during recalescence is sufficient for retrograde melting of the silicon nanoparticle or not.

We have performed MD simulations to evaluate the melting temperature of silicon nanoclusters comprising a maximum of 8970 atoms. The result has acceptable agreement with the previous study[58, 44]. The result also reveals the dependence of melting temperature on heating rate. Using Stillinger-Weber potential, we have obtained two completed curve with heating rate of 0.01 K/fs and 0.001 K/fs as shown in Figure 15.

Diameter $[nm]$	number of atoms	$T_{melting}[K]$ 0.01 K/fs	$T_{melting}[K]$ 0.001 K/fs
2.0	205	1025($\pm$12.5)	950($\pm$12.5)
2.5	416	1200($\pm$12.5)	1150($\pm$10)
3.0	702	1350($\pm$12.5)	1275($\pm$10)
3.5	1126	1400($\pm$12.5)	1300($\pm$10)
4.0	1677	1450($\pm$12.5)	1350($\pm$12.5)
5.0	3275	1525($\pm$10)	1450($\pm$12.5)
6.0	5638	1625($\pm$12.5)	1550($\pm$12.5)
7.0	8970	1700($\pm$12.5)	1610($\pm$10)
Bulk	∞	1795	1720
Bulk(experiment)	∞	1683	1683

Table 2: Dependence of melting points on cluster size and heating rate. For experimental data see reference[58, 44]

Figure 16 illustrates the average potential energy (PE) per atom of Si nanoparticle with 1677

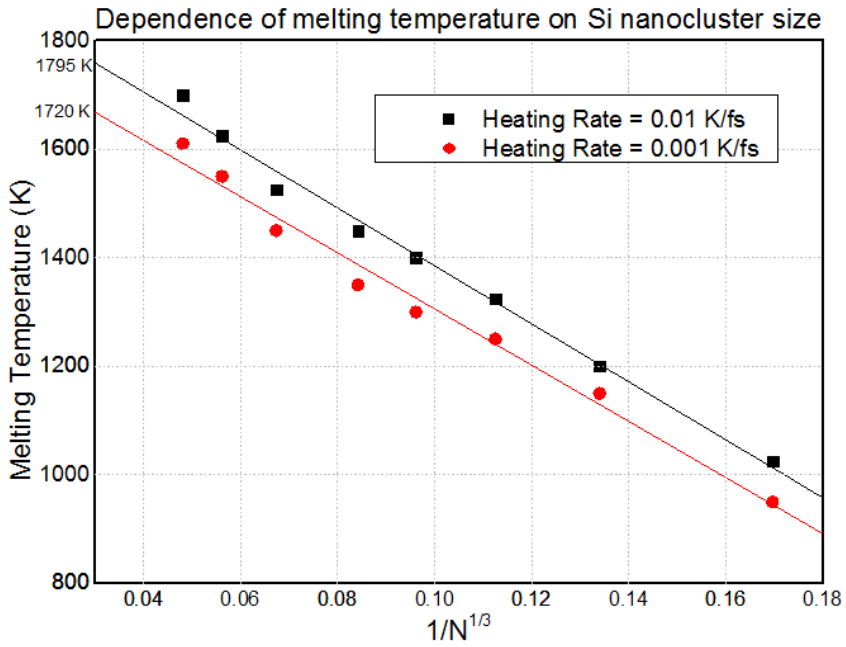

Figure 15: Dependence of melting temperature on heating rate. Extrapolation of linear fitting is 1795 K and 1720 K for two heating rates respectively.

atoms as a function of temperature (T) during heating and cooling process with heating and cooling rate 0.0001 K/fs. The melting transition is clearly identified by a rapid increase in potential energy. The melting point for 4nm-sized cluster with 0.0001 K/fs is 1263 K. Due to the fast cooling rate, the clusters remain amorphous after cooling down. The points of intersection of linear fitting lines can be considered as the melting points in heating and cooling process. It can be seen that the Si nanoparticle undergoes the undercooling process.

6.1.2 Silver induced crystallization

To provide quantitative insight into the cooling and crystallization processes, we plotted the time evolution of the temperature and the fraction of disordered atoms separately for Si and Ag atoms. In Figure 17(g), blue and red curves represent Si and Ag respectively. In the plotted case, the system comprised 1677 Si atoms, 350 Ag atoms and 1000 Ar atoms, and the initial temperatures are 3349.9 K for Si cluster, 1895.3 K for Ag atoms and 287.6 K for Ar atoms. The temperature of Si and Ag reduced dramatically to 2250 K and 500 K respectively, at the very beginning of the simulation. Later on, the temperature of Si still decreased exponentially to 1000 K and the cluster made a transition from liquid to an amorphous solid state. At the time t = 40.0 ns, crystallization started as the Ag atoms started aggregating inside the Si cluster. We noticed that at first silver silicide starts forming in two different

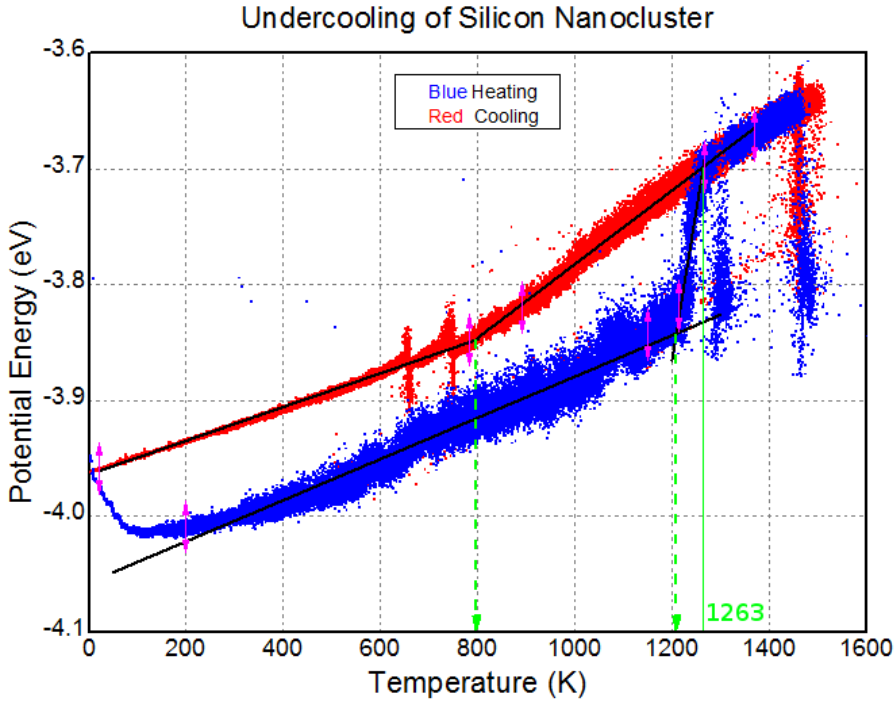

Figure 16: Undercooling of Si nanoparticle. The points of intersection of linear fitting lines are 800K for cooling process and 1200 for heating process.

regions inside of the silicon cluster, as shown in Figure 17(b). As the second step, the silver silicide phase which is in the center of the cluster diffuses to the Ag sub-shell on the surface and forms a single Ag nanocluster. The Si cluster is heated up by the energy released during the Ag coalescence and forms a bicrystalline structure within 2.0 ns. After the crystalline structure formed, the condensed Ag cluster adheres to the surface of Si cluster for 2.5 ns and eventually leaves the Si cluster. Some gas phase condensed Ag clusters incidentally land on or penetrate into the Si cluster afterwards, however the bicrystalline structure of the Si cluster remains as shown in Figure 17(f). Figure 17(h) quantitatively reveals the aggregation, diffusion and coalescence process during the simulation, "In vacuum" represents isolated Ag atoms in gas phase and "Only Ag" indicates condensed Ag clusters away from the Si nanocluster. "$N_{Ag} > N_{Si}$" means Ag atoms with more bonds to Ag than Si, and "$N_{Ag} > N_{Si}$" vice versa. Initially isolated Ag atoms form dimers and trimers before landing on the Si cluster, and only 10 percent of Ag atoms involves in crystallization process.

One reference simulation with 1677 Si atoms, 1112 Ar atoms and the absence of silver atoms, can be used to compare with the experimental result. As shown in Figure18, the Si nanoparticle remains amorphous after cooling in Ar atmosphere and undergoes a phase transition from liquid phase to solid phase at the temperature T = 860 K, which is also

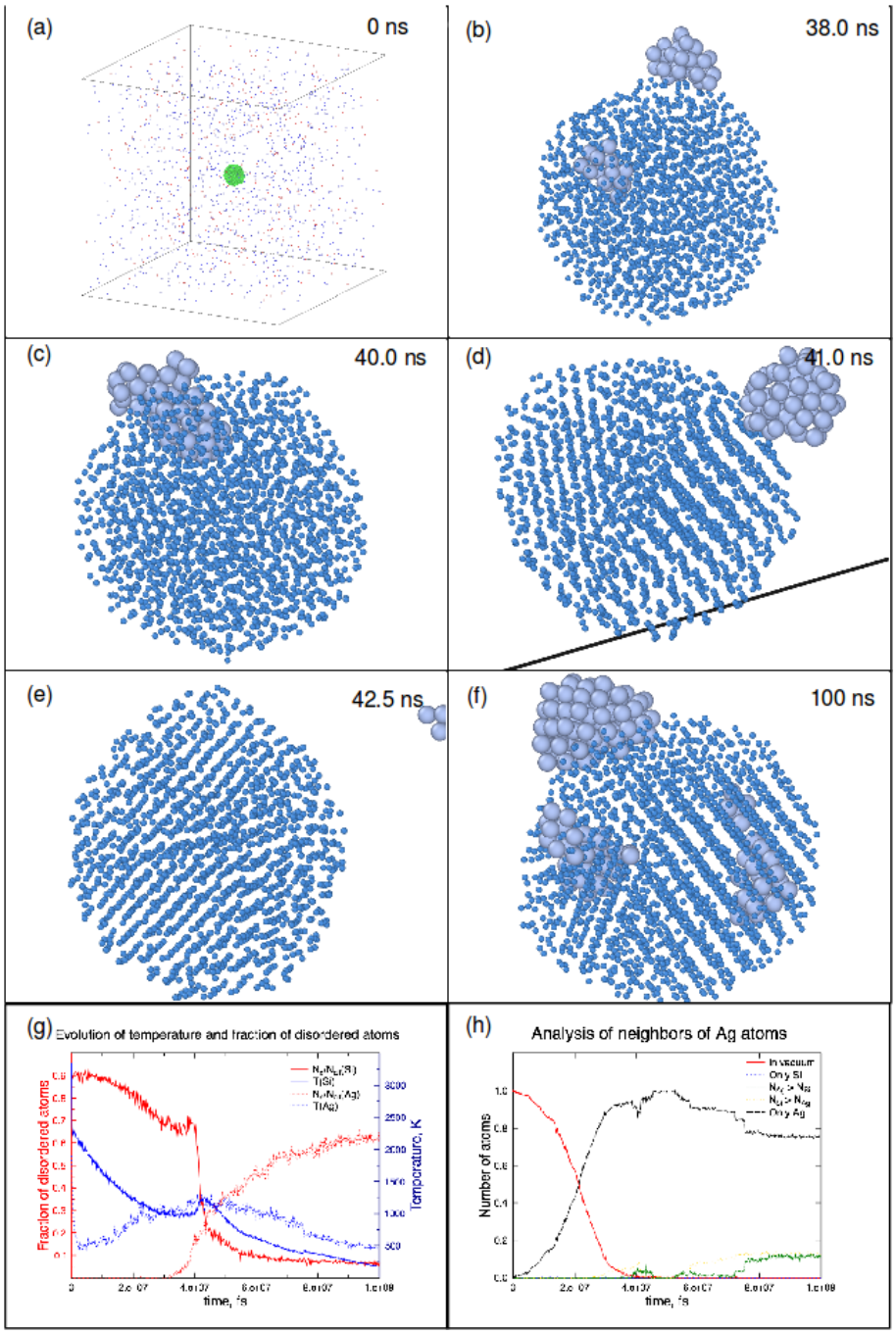

Figure 17: polycrystallized case: (a) Initial state of MD simulation; (b) Metastable silver silicide and Ag sub-shell; (c) Ag coalescence on the surface of Si cluster; (d) Bicrystalline structure formation; (e) Ag nanoparticle leaves Si cluster; (f) Final state of MD simulation; (g) Evolution of temperature and fraction of disordered atoms; (h) Analysis of neighbours of Ag atoms.

consistent with the result in previous section. The fraction of amorphous atoms generally reduces to 0.33. One unexpected result is that the final temperature of the Si nanoparticle is

much lower than 300 K (about 50 K).

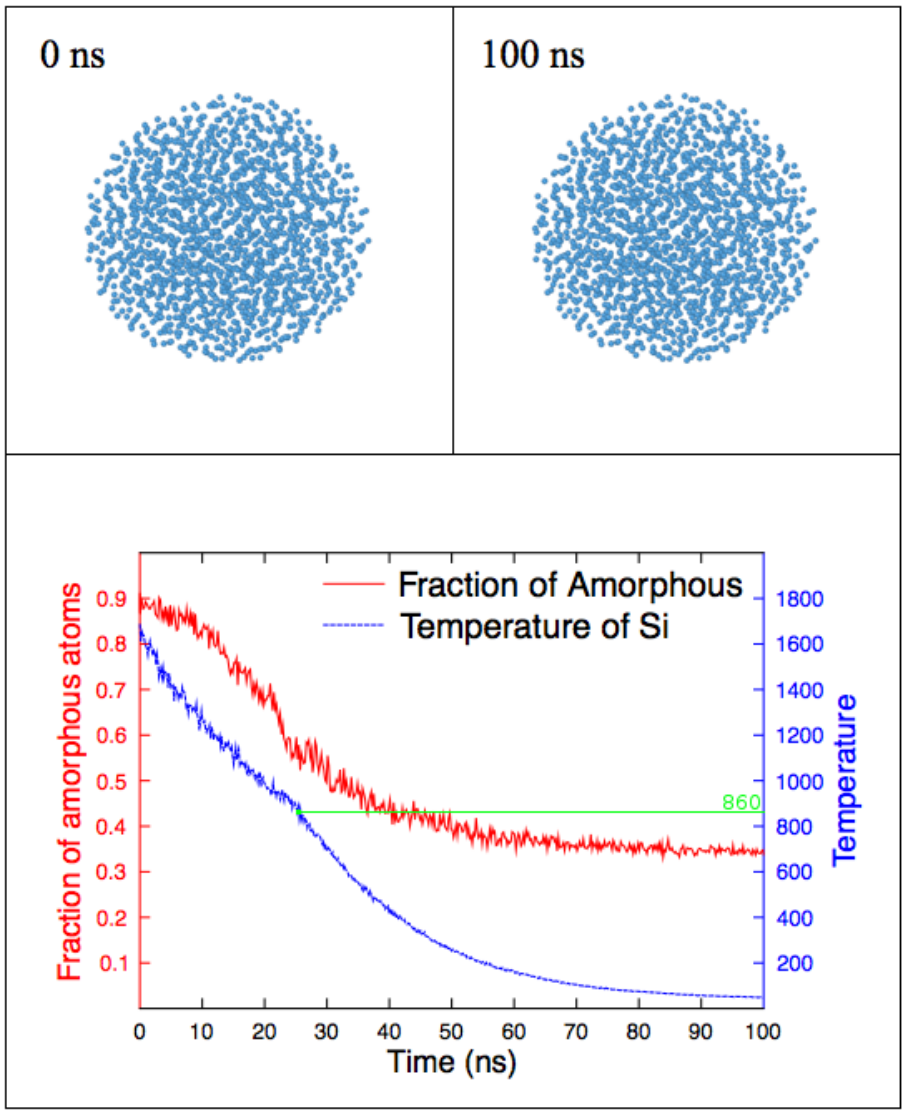

Figure 18: Reference simulation

Another similar simulation whose initial temperature of Si atoms is 2500 K, indicates that the initial temperature of the Si cluster has only minor effect on the crystallisation process. In this case, silver atoms initially aggregate separately inside the silicon cluster as small particles (15 20 atoms) as shown in Figure 19(a) and follows with further coalescence to form two large eutectic phases as shown in Figure 19(b). The coalescence and departure of the silver particles happens within 0.8 ns, which is not sufficiently long for the formation of nucleation of crystalline phase. Eventually, the silicon cluster remains in amorphous phase with three silver sub-shells, as shown in Figure 19(e).

One group of simulations containing twenty runs were conducted to gain the insight into

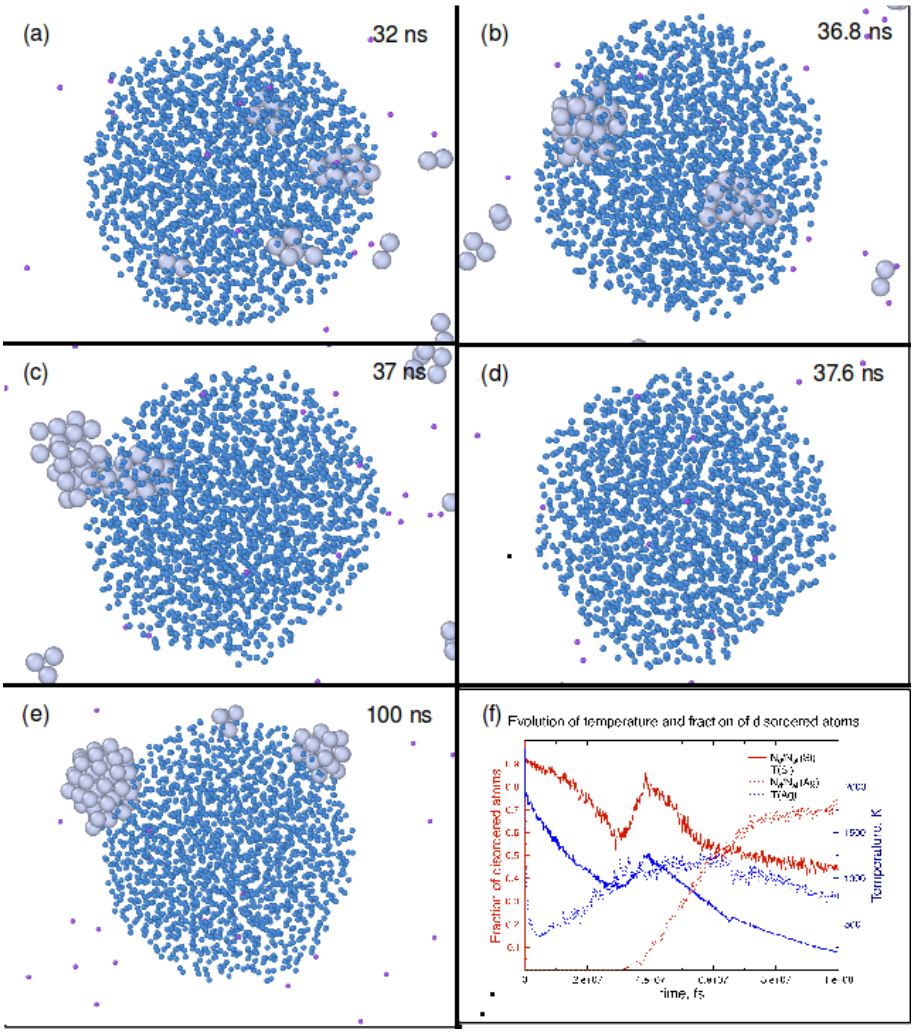

Figure 19: Noncrystalline case: a) Silver atoms form four small particles inside the silicon cluster; b) The small silver particles merge as two large eutectic phases; c) The coalescence occurs near the cluster surface; d) The silver particle leaves the silicon cluster without inducing crystallisation; e) Finally, the silicon cluster remains amorphous with silver subshells; f) Evolution of temperature and fraction of disordered atoms: form 30 ns to 38 ns, the temperature of the silicon cluster increases from 700 K to 1200 K.

the statistical behaviours. Each run has the identical numbers of atoms (1677 Si atoms, 112 Ag atoms, 1000 Ar atoms) but the different initial positions and velocities for each atom. We note that four types of processes occur: 1) non-crystalline structure Si cluster with Ag sub-shell; 2) crystallization happens but Si cluster is remelted; 3) Stable polycrystalline structure cluster with Ag aggregate inside Si cluster; 4) Stable single crystalline structure The histogram of the occurrence frequency of each type which is shown in Figure 4 indicate that the probability of crystallisation is 45 percent. Among these simulations, we note that one simulation result in single crystalline structure induced by only three Ag atoms, as shown in Figure 5(a). The reference simulations with 1112 Ar atoms but no Ag atom indi-

cate that homogeneous nucleation of crystalline seed is scarcely possible due to relatively high energy barrier and high cooling rate (35 K/ns)[19]. The growth of single crystalline silicon requires long time annealing at the temperature exceeding 1000K and the critical cooling rate($< 30 \times 10^{-9} K/ns$)[26]. Therefore, the crystallization in this case is induced by the "bond-weakening effect" of Ag atoms. As shown in Figure 5(b), an intrinsic single crystal silicon nanocluster is left after the separation of Ag atoms and Si cluster. We also note that after the crystallization finished, Ag atoms start to aggregate inside the silicon cluster(Figure 5(c)) and destroy the crystalline structure again(Figure 5(d)).

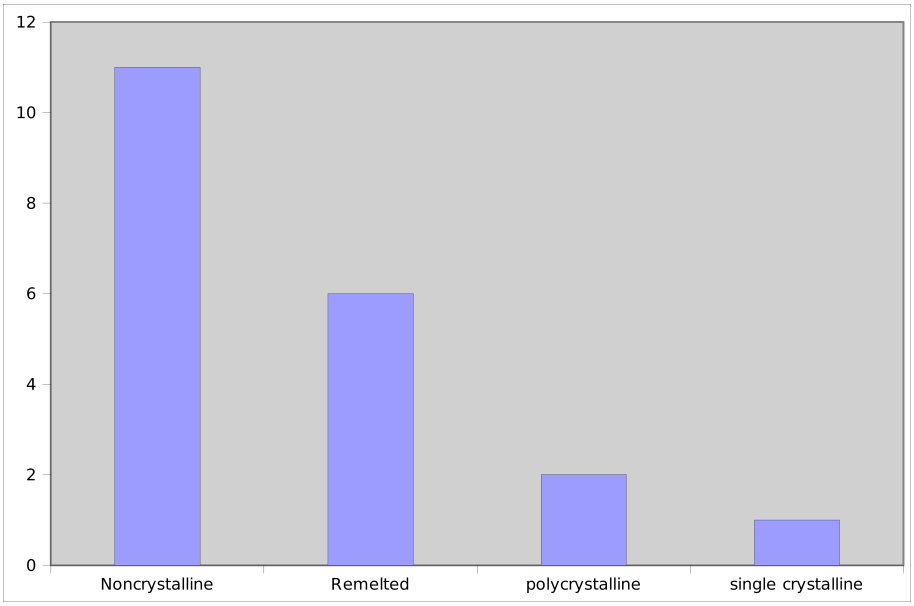

Figure 20: Occurrence frequency of each type.

Due to the presence of defects, the total potential energy (PE) of the amorphous Si nanoparticle is higher than the crystallized Si nanoparticles. This difference of potential energies will release and transfer to kinetic energy in half during the crystallization (the other half introduced as thermal expansion). As shown in Figure22, two structure of the Si particles is picked out from one simulation. One is the amorphous structure before crystallization and the other is polycrystalline after crystallization. The two structures are cooled to 1K with very fast cooling rate (0.01 K/fs). By calculating the difference of the potential energies and simply dividing the atomic heat capacity of silicon ($2.05126 \times 10^{-4} eV/K$ per atom), one can estimate the temperature change during the crystallization:

In a new set of simulations, we use smaller time step (the maximum time step = 1.079 fs) to maintain the total energy conservation of the system. Figure 23 (b) shows the total energy drift per atom during the simulation, which is separated into "linear region" and "exponential region". This is due to the initial gas phase Ag atoms having strong coupling

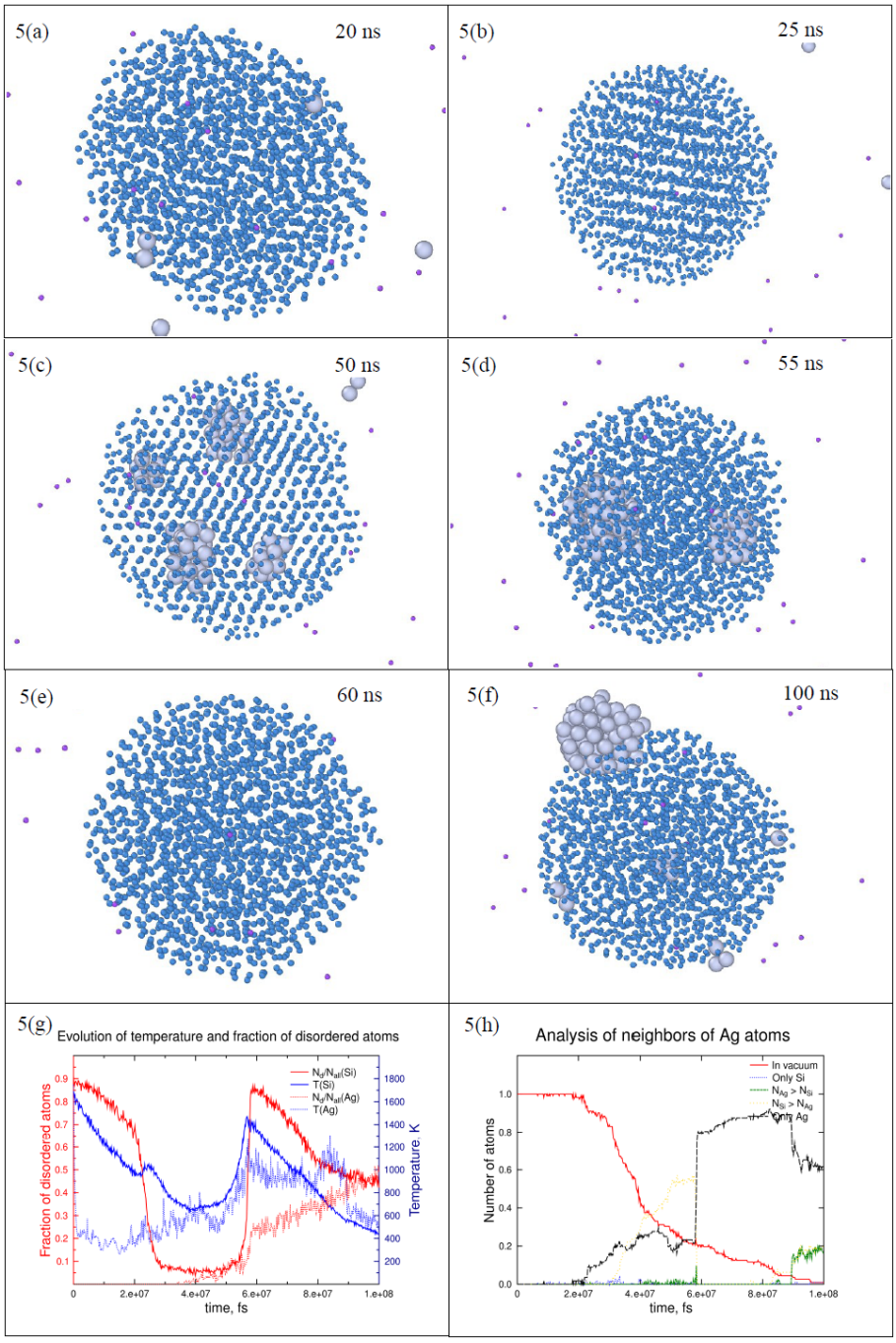

Figure 21: single-crystallized case: (a) Three Ag atoms penetrate in the Si cluster; (b) Single crystalline without the present of Ag atoms; (c) Ag atoms aggregate inside crystallized Si cluster; (d) The cluster is reheated by the energy released by the coalescence of eutectic phase and crystalline structure is destroyed; (e) Ag nanoparticles were separated out as eutectic temperature is exceeded; (f) Relatively large Ag nanoparticles adhere on the surface of cooled amorphous Si cluster; (g) Evolution of temperature and fraction of disordered atoms; (h) Analysis of neighbours of Ag atoms.

PE of Amorphous$[eV]$	PE of Polycrysalline$[eV]$	Difference$[eV]$	Temperature change$[K]$
-6559.889	-6795.929	236.04	324

Table 3: Estimated temperature change of Si nanoparticle during crystallization

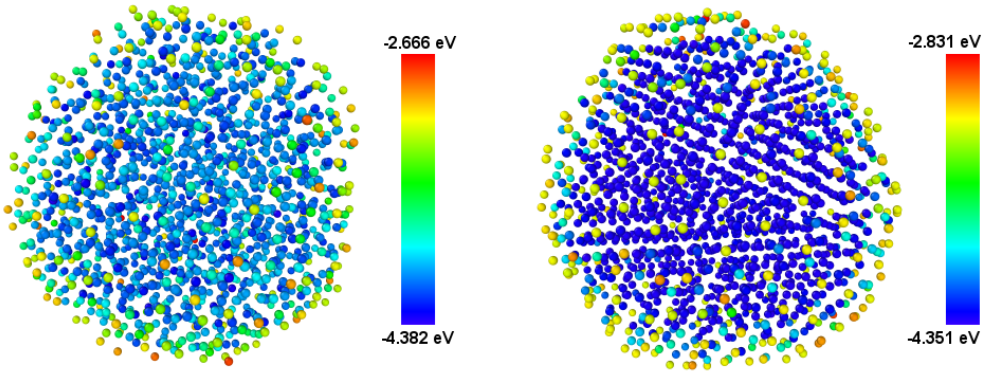

Figure 22: Amorphous structure and polycrystalline structure after cooling to 1K. The colour coding is the potential energy for each atom.

with Ar atmosphere and the coupling becoming weaker after the Ag atoms aggregate into small clusters and are condensed on the Si nanocluster. The temperature change during the crystallization is 267 K and the highest temperature is 1267 K. From previous reference simulation, the melting point for 4 nm sized Si nanocluster is 1263 K for 0.0001 K/fs heating rate. If we approximately consider the heating process during the crystallization is linear, the estimated heating rate is $4.85 \times 10^{-5} K/fs$ which is lower than 0.0001 K/fs. Therefore, the Si nanocluster is remelted during the crystallization.

Figure 24 shows the detailed interaction between Ag atoms and Si naocluster: there are three Ag clusters initially existing inside the Si nanocluster, and these clusters have relatively high mobility and aggregate as one large eutectic phase. After the crystallization, Ag cluster stays inside the Si nanocluster.

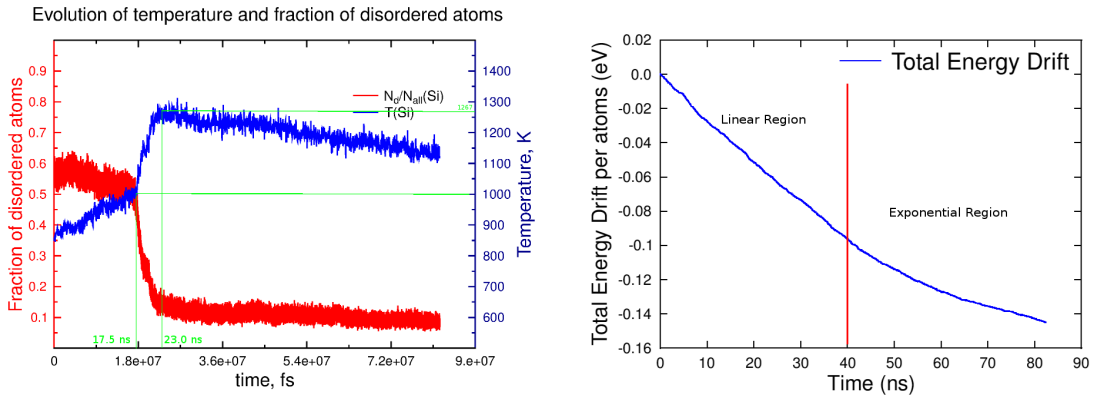

Figure 23: (a) Increase of the temperature during the crystallization is 267 K and the estimated heating rate is $4.85 \times 10^{-5} K/fs$.(b) Total energy drift of the whole system per atom during simulation, which can be separated into linear region and exponential region

The observed behaviour of silicon and silver interaction leading to the metal induced crystallization of silicon nanoparticle can be explained by the energy balance: energy release during formation of new bonds and its consumption during the phase transitions. All the crystallized cases are happened at the temperature of 1000 K which is corresponding to the temperature at which the Ag-Si eutectic alloy forms. Since thermal conductivity of silicon is relatively high 1.3 $Wcm^{-1}K^{-1}$ and the diameter of silicon cluster is 4 nm, the whole cluster can be regarded as homogeneous system. This is also confirmed by checking the kinetic energy for each atom. The potential energy released during the crystallization process is sufficient to remelt the nanocluster

In principle, free atoms in a-Si matrix could reduce the Gibbs energy of the system by (a) crystallization; (b) dissolving into the metal layer; (c) reacting with the metal to form silicides; (d) diffusing to sites of low energy (as grain boundaries in the metal). In the specific system considered in this work, the formation of any silicide can be excluded as shown in supported animation. The diffusion and dissolution of Si in Ag nanoparticle are negligible at the certain temperature (< 1108 K). Furthermore, for very small Ag nanoparticles, no grain boundaries could work as low energy sites. As a result, only one option for the interfacial free Si atoms to lower the system Gibbs energy is to crystallize at the interface with Ag.

The simulations have good agreement with the experimental result. The mechanism behind can not be simply explained by MIC or retrograde melting individually, since retrograde melting can only explain the high mobility of eutectic phase, but not necessarily results

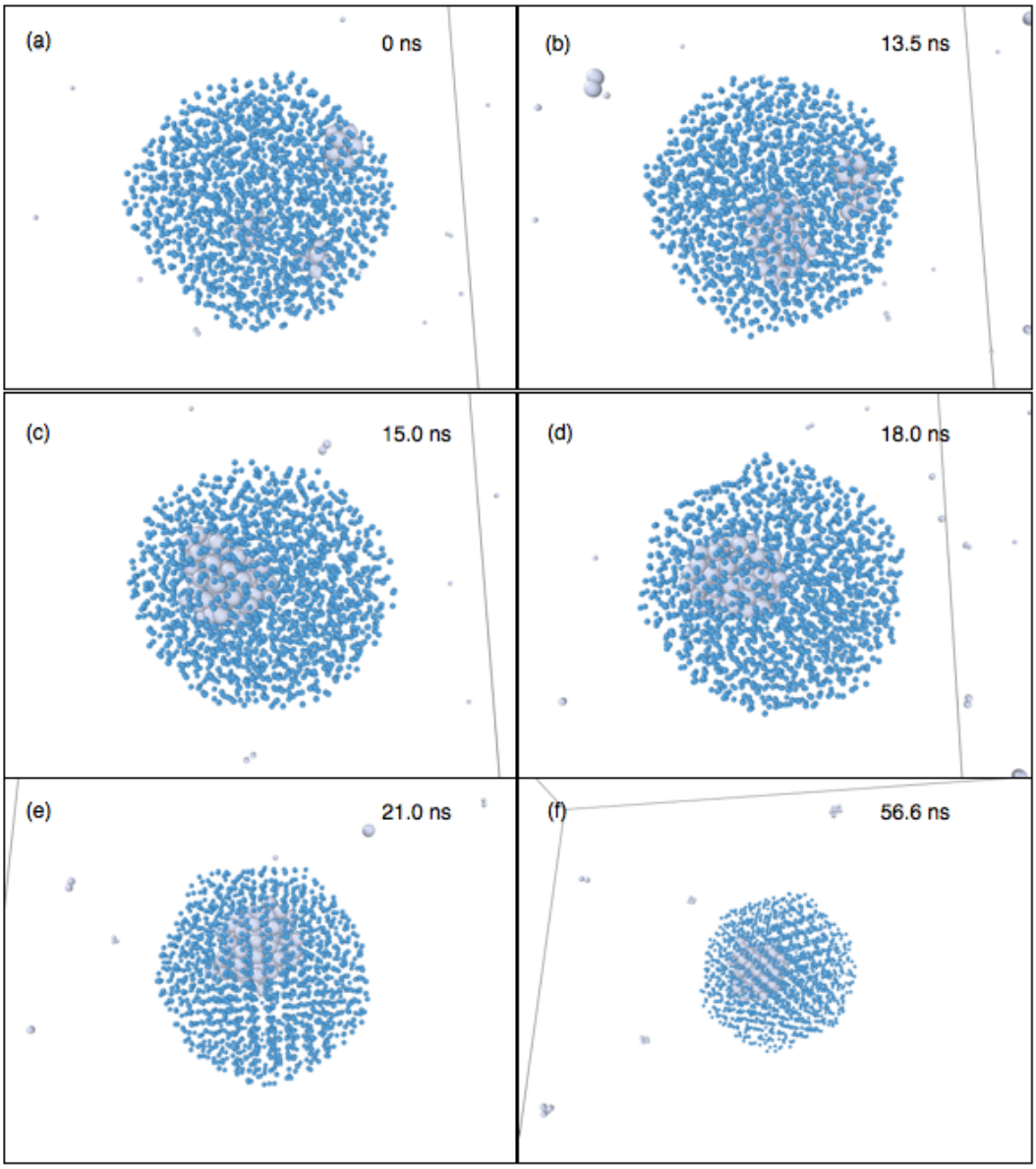

Figure 24: MD Simulation to model the interaction of Ag cluster inside Si cluster

in crystallization. The amorphous-to-crystalline phase transformation of silicon invariably requires about 1000 K[33], which is consistent for all simulations.

7 Conclusions

Complexity of multi-elemental nanosystems may lead to very promising applications, but also can be very difficult to model. MD simulation become a powerful tool to study this kind of systems. In this work, the MD simulations of Ag-Si nanocluster are presented as a good example. Various initial conditions and combinations of each atom type provide a detailed insight for the behaviour of this metal-semiconductor nanosystem.

The crystallization temperature of the Si nanocluster is 1000 K which is independent of the initial conditions of the system. The Ag atoms have relatively high mobility in amorphous silicon structure and can aggregate inside the Si cluster and trend to form large eutectic phase. The presence of Ag atoms is essential for the crystallization process and the energy released during the crystallization process can remelt the Si nanocluster. However, the number of nanograins is independent of the number of eutectic phases. The simulation system is somewhat smaller than the experimental system, thus the crystallization process occurs in nanosecond scale.

In conclusion, Ag atoms is introduced as heterogeneous seeds for crystallization, the retrograde melting process provide a high mobility for Si atom surrounding the eutectic phase. These free Si atoms can work as the initiation of the nucleation of crystallization.

References

[1] N. Tanaguchi. On the basic concept of 'nano-technology'. *Proc. Intl. Conf. Prod. Eng. Tokyo: JSPE*, 1974.

[2] G. Binning and H. Rohrer. Scanning tunneling microscopy. *IBM J. Res. Dev.*, 30:355, 1986.

[3] S. C. O'Brien R. F. Curl H. W. Kroto, J. R. Heath and R. E. Smalley. C60-buckminsterfullerene. *Nature*, 318:162, 1985.

[4] C. P. Poole Jr. and F. J. Owens. Introduction to nanotechnology. *John Wiley Sons. Inc.*, 2003.

[5] V. Ya. Shevchenko and A. E. Madison. Structure of nanoparticles: I. generalized crystallography of nanoparticles and magic numbers. *Glass Physics and Chemistry*, 28:40–43, 2002.

[6] H. F. Tibbals G. L. Hornyak, J. Dutta and A. K. Rao. Introduction to nanoscience. *CRC Press*, 2008.

[7] J. Stairs M. N. Blom, D. Schooss and M. M. Kappes. Experimental structure determination of silver cluster ions (ag-n(+),19 <= n <= 79). *J. Chem. Phys.*, 124, 24, 244308, 2006.

[8] A. Lorke P. Petroff and A. Imamoglu. Epitaxially self-assembled quantum dots. *Physics Today*, 54:46–52, 2001.

[9] A. C. Dillon P. A. Parilla G. L. Hornyak, L. Grigorian and M. J. Heben. A temperature window for chemical vapor deposition growth of single walled carbon nanotubes. *Journal of Physical Chemistry B*, 106:2821–2825, 2002.

[10] C. L. De Castro and B. S. Mitchell. Synthesis, functionalization and surface treatment of nanoparticles. *American Scientific Publishers, Stevenson Ranch, CA*, 2002.

[11] Douglas B. Chrisey and Graham K. Hubler. Pulsed laser deposition of thin films. *John Wiley Sons*, 1994.

[12] Y. Ando and M. Ohkohchi. Production of ultrafine powder of p-sic ny arc discharge. *Journal of Crystal Growth*, 60:147–149, 1982.

[13] S. L. Gafner and Yu. Ya. Gafner. Analysis of gas-phase condensation of nickel nanoparticles. *Journal of Experimental and Theoretical Physics*, 107:712–722, 2008.

[14] http://www.oaresearch.co.uk/oaresearch/cluster/.

[15] N. W. Ashcroft and N. D. Mermin. Solid state physics. *Thomson Learning*, 1976.

[16] F. Scholz. http://www-opto.e-technik.uni-ulm.de/lehre/cs/index.html.

[17] J. E. Greene and L. Mei. Metal-induced crystallization of r.f. sputtered a-si thin films. *Thin Solid Film*, 34:27–30, 1976.

[18] W. D. Callister Jr. and D. G. Rethwisch. Fundamentals of materials science and engineering- an integrated approache. *John Wiley Sons, Inc.*, 2008.

[19] T. J. Konno and R. Sinclair. Metal-contact-induced crystallization of semiconductors. *Materials Science and Engineering A-Structural Materials Properties Microstructure and Processing*, 179:426–432, 1994.

[20] O. Nast and S. R. Wenham. Elucidation of the layer exchange mechanism in the formation of polycrystalline silicon by aluminum-induced crystallization. *J. Appl. Phys.*, 88:124–132, 2000.

[21] M. Gjukic M. Scholz and M. Stutzmann. Silver-induced layer exchange for the low-temperature preparation of intrinsic polycrystalline silicon films. *Applied Physics Letters*, 94:012108, 2009.

[22] L. P. H. Jeurgens Z. M. Wang, J. Y. Wang and E. J. Mittemeijer. Thermodynamics and mechanism of metal-induced crystallization in immiscible alloy systems: Experiments and calculations on al/a-ge and al/a-si bilayers. *Physical Review B*, 77:045424, 2008.

[23] U. Gnauert W. Schroter M. Seibt, S. Buschbaum and D. Oelgeschlager. Nanoscale observation of a grain boundary related growth mode in thin film reactions. *Physical Review Letters*, 80:774–777, 1998.

[24] T. J. Konno and R. Sinclair. Metal-mediated crystallization of amorphous-silicon in silicon silver layered systems. *Philosophical Magazine B-Physics of Condensed Matter Statistical Mechanics Electronic Optical and Magnetic Properties*, 71:163–178, 1995.

[25] C. Jeong M. Jeon and K. Kamisako. Tin induced lateral crystaliization of amorphous silicon thin films. *IEEE Tran. Electron Devices*, 46:78–82, 1999.

[26] K. U. M. Kumar and M. G. Krishna. Chromium-induced nanocrystallization of a-si thiin films into the wurtzite structure. *J. Nanomater.*, pages 736534–1–6, 2008.

[27] M. G. Krishna A. K. Bhatnagar K. U. M. Kumar, R. Brahma and G. Dalba. An optical study of ni induced crystallization of a-si thin film. *J. Phys. Condens. Matter*, 49:496208–1–11, 2007.

[28] H. S. Kwok Z. Jin, G. A. Yeung and M. Wong. Nickel induced crystallization of amorphous silicon thin film. *J. Appl. Phys.*, 84:194–200, 1998.

[29] J. L. Murray and A. L. McAlister. Binary alloy phase diagrams. *American Society of Metals*, 1986.

[30] L.P.H. Jeurgens Z. M. Wang, J. Y. Wang and E. J. Mittemeijer. Tailoring the ultra-thin al-induced crystallization temperature of amorphous si by application of interface thermodynamics. *Physical Review Letters*, 100:125503, 2008.

[31] J. A. Bucaro and H. D. Dardy. High-termperature brillouin scattering in fused quartz. *Journal of Applied Physics*, 45:5324–5329, 1974.

[32] A. Hiraki. A model on the mechanism of room-temperature interfacial intermixing reaction in various metal-semiconductor couples - what triggers the reaction. *J.Electrochem.Soc.*, 127:2662–2665, 1980.

[33] L.P.H. Jeurgens Z. M. Wang, J. Y. Wang and E. J. Mittemeijer. Fundamental of matal-induced crystallization of amorphous semiconductors. *Advanced Engineering Materials*, 11, 2009.

[34] D. H. Speidel and R. H. Nafziger. Retrograde melting in the system mg-fe-si-o. *Science*, 152:1367–1368, 1966.

[35] S. Wagner and D. A. Rigney. Binary-systems involving catatectic reaction solid 1 cooling reversible heating solid 2 + liquid. *Metallurgical Transactions*, 5:2155–2160, 1974.

[36] M. I. Bertoni S. Hudelson S. Bernardis M. A. Marcus S. C. Fakra D. P. Fenning, B. K. Newman and T. Buonassisi. Local melting in silicon driven by retrograde solubility. *Acta. Materialia*, 61:4320–4328, 2013.

[37] A. A. Istratov M. D. Pickett M. A. Marcus B. Lai Z. Cai S. M. Heald T. Buonassisi, M. Heuer and E. R. Weber. Transition metal co-precipitation mechanisms in silicon. *Acta Materialia*, 55:6119–6126, 2007.

[38] http://www.crct.polymtl.ca/fact/phase$_diagram.php?file = AgSi.jpgdir = SGTE.$

[39] S. Kawanishi T. Yoshikawa, K. Morita and T. Tanaka. Thermodynamics of impurity elements in solid silicon. *Journal of Alloys and Compounds*, 490:31–41, 2010.

[40] P. Grammatikopoulos F. Djurabekova K. Nordlund C. Cassidy, V. Singh and M. Sowwan. Inoculation of silicon nanoparticles with silver atoms. *Scientific Reports*, 3:3083, 2013.

[41] L. Verlet. Computer experiments on classical fluids .i. thermodynamical properties of lennard-jones molecules. *Physical Review*, 159:98, 1967.

[42] R. W. Hockney and J. W. Eastwood. Computer simulation using particles. *Adam Hilger, Bristol*, 1988.

[43] D. Knuth. Computers typesetting: Reading, ma. *Addison-Wesley,*, 1984.

[44] Z. H. Cao H. M. Lu, P. Y. Li and X. K. Meng. Size-, shape-, and dimensionality-dependent melting temperatures of nanocrystals. *Journal of Physical Chemistry C*, 113:7598–7602, 2009.

[45] L. Verlet. Computer experiments on classical fluids .2. equilibrium correlation functions. *Physical Review*, 165:201, 1968.

[46] P. H. Berens W. C. Swope, H. C. Andersen and K. R. Wlison. A computer-simulation method for the calculation of equilibrium-constants for the formation of physical clusters of molecules - application to small water clusters. *Jounrnal of Chemical Physics*, 76:637–649, 1982.

[47] H. J. C. Berendsen. Transport properties computed by linear response through weak coupling to a bath. *Computer Simulations in Materials Science*, Kluwer, 1991.

[48] S. Nosé. A molecular dynamics method for simulations in the canonical ensemble. *Mol. Phys.*, 52:255–268, 1984.

[49] W. G. Hoover. Canonical dynamics: equilibrium phase-space distributions. *Physical Review*, 31:1695–1697, 1985.

[50] A. DiNola H. J. C. Berendsen, J. P. M. Postma and J. R. Haak. Molecular dynamics with coupling to an external bath. *Journal of Chemical Physics*, 81:3684–3690, 1984.

[51] M. Parrinello and A. Rahman. Polymorphic transitions in single crystals: A new molecular dynamics method. *Journal of Applied Physics*, 52:7182–7190, 1981.

[52] S. Nosé and M. L. Klein. Constant pressure molecular dynamics for molecular system. *Mol. Phys.*, 50:1055–1076, 1983.

[53] J. E. Jones. On the determination of molecular fields. ii. from the equation of state of a gas. *Proceedings of the Royal Society of London. Series A, Containing Papers of a Mathematical and Physical Character*, 106:463–477, 1924.

[54] I. R. Mcdonald and K. Singer. Calculation of thermodynamic properties of liquid argon from lennard-jones parameters by a monte carlo method. *Discussions of the Faraday Society*, page 40, 1967.

[55] F. H. Stillinger and T. A. Weber. Computer-simulation of local order in condensed phases of silicon. *Physical Review B*, 31:5262–5271, 1985.

[56] M. I. Baskes S. M. Foiles and M. S. Daw. Embedded-atom-method functions for the fcc metals cu, ag, au, ni, pd, pt, and their alloys. *Physical Review B*, 33:7983–7991, 1985.

[57] K. Nordlund and R. S. Averback. Points defect movement and annealing in collision cascades. *Physical Review B*, 56:2421–2431, 1997.

[58] K. C. Fang and C. I. Weng. An investigation into the melting of silicon nanoclusters using molecular dynamics simulations. *Nanotechnology*, 16:250–256, 2005.